

# Resummations in QCD hard-scattering at large and small $x$

Nikolaos Kidonakis<sup>1</sup>, Agustín Sabio Vera<sup>2</sup>, Philip Stephens<sup>1</sup>

<sup>1</sup>*Kennesaw State University, 1000 Chastain Rd. # 1202, Kennesaw, GA 30144, USA*

<sup>2</sup>*Physics Department, Theory Division, CERN, CH-1211 Geneva 23, Switzerland*

We discuss different resummations of large logarithms that arise in hard-scattering cross sections of quarks and gluons in regions of large and small  $x$ . The large- $x$  logarithms are typically dominant near threshold for the production of a specified final state. These soft and collinear gluon corrections produce large enhancements of the cross section for many processes, notably top quark and Higgs production, and typically the higher-order corrections reduce the factorization and renormalization scale dependence of the cross section. The small- $x$  logarithms are dominant in the regime where the momentum transfer of the hard sub-process is much smaller than the total collision energy. These logarithms are important to describe multijet final states in deep inelastic scattering and hadron colliders, and in the study of parton distribution functions. The resummations at small and large  $x$  are linked by the eikonal approximation and are dominated by soft gluon anomalous dimensions. We will review their role in both contexts and provide some explicit calculations at one and two loops.

## 1 Introduction

Particle physics in high-energy hadron colliders depends crucially on our ability to calculate cross sections to an ever increasing theoretical accuracy, which is achieved by the incorporation of higher-order corrections. Hard-scattering cross sections in perturbative QCD obey factorization theorems [1] that play a key role in the calculation of these corrections. Typically, the cross section for a process involving the collision of two hadrons (proton-antiproton at the Fermilab Tevatron or proton-proton at the CERN LHC) into a specified final state can be described as a convolution of non-perturbative parton distribution functions that describe the parton content of the hadron, and a partonic cross section that can be calculated order-by-order in perturbation theory. The short-distance partonic cross section involves the scattering of quarks and gluons. The partonic processes are of the form

$$f_1(p_1) + f_2(p_2) \rightarrow F(p) + X, \quad (1)$$

where  $f_1$  and  $f_2$  represent partons (quarks or gluons),  $F$  represents an observed system in the final state, such as a top quark or a jet or a Higgs boson, and  $X$  represents any additional final-state particles. The factorization is described schematically by

$$\sigma_{h_1 h_2 \rightarrow F} = \sum_f \int dx_1 dx_2 \phi_{f_1/h_1}(x_1, \mu_F) \phi_{f_2/h_2}(x_2, \mu_F) \hat{\sigma}_{f_1 f_2 \rightarrow F}(s, t, u, \mu_F, \mu_R), \quad (2)$$

where  $\sigma_{h_1 h_2 \rightarrow F}$  is the physical cross section (total or differential) for the production of final state  $F$  in the scattering of hadrons  $h_1$  and  $h_2$ ,  $\phi_{f_i/h_i}$  is the distribution function for parton  $f_i$  with momentum fraction  $x_i$  of hadron  $h_i$ , and  $\hat{\sigma}_{f_1 f_2 \rightarrow F}$  is the partonic cross section. The collinear singularities are factorized in a process-independent manner and absorbed into the parton distribution functions which are dependent on the factorization scale  $\mu_F$ . The physical cross section is in principle independent of the factorization scale  $\mu_F$  and the renormalization scale  $\mu_R$ , but in practice there is a strong dependence because we truncate the infinite perturbative series at finite order (typically next-to-leading-order (NLO) or next-to-next-to-leading-order (NNLO) in the strong coupling  $\alpha_s$ ). The parton-level cross section explicitly involves the standard kinematical invariants,  $s = (p_1 + p_2)^2$ ,  $t = (p_1 - p)^2$ ,  $u = (p_2 - p)^2$ , formed from the 4-momenta of the particles in the hard scattering.

Near threshold, i.e. when the energy of the incoming partons is just sufficient to produce a final state without additional radiation, the production cross section receives significant corrections from large- $x$  logarithms [2–5]. These logarithms arise from incomplete cancellations between virtual terms and terms that describe soft-gluon emission. Since near threshold any additional radiation has to be soft, the large- $x$  logarithms are especially important in that kinematical region. Large- $x$  resummation depends critically on the color structure of the process [4, 6–8] as well as the kinematics [4, 9].

Small- $x$  logarithms arise when the perturbative scales characterizing the hard-subprocess are much smaller than the total collision energy. In this case resummation of logarithms of the form  $\ln(1/x)$  becomes important. When the transverse scales of the outgoing scattered particles are similar and large this resummation can be described by the Balitsky-Fadin-Kuraev-Lipatov (BFKL) evolution equation [10–14]. This equation is a linear integral equation which leads to an exponential rise of the cross section. The slope of this rise can be interpreted as a perturbative construction of the QCD Pomeron. This Pomeron is considered the mediator of many QCD diffractive processes, such as diffractive vector meson production.

The conditions by which the BFKL evolution should be valid are satisfied by jet production with large rapidity gaps. Phenomenological studies of this process with the summation of the terms  $\alpha_s^n \ln^n(1/x)$  (leading-order kernel) are not very predictive since the value of the coupling is a free parameter and the Regge energy scale, a sort of factorization scale at high energies, can only be fixed at higher orders. Inclusion of the next-to-leading order corrections,  $\alpha_s^{n+1} \ln^n(1/x)$  [15, 16], brings the predictions in closer agreement with data.

In the next section we discuss large- $x$  resummation and finite-order expansions of the resummed cross section through next-to-next-to-next-to-leading order (NNNLO). In Section 3 we present some applications of large- $x$  resummation to various hard-scattering pro-

cesses, namely top-antitop pair production, single top quark production,  $W$ -boson production at large transverse momentum, and Higgs boson production via  $b\bar{b} \rightarrow H$ . In Section 4 we present typical one-loop and two-loop calculations in the eikonal approximation that are needed in resummations for processes with massive quarks, such as heavy quark pair production. Section 5 discusses small- $x$  resummation and applications of BFKL. We conclude in Section 6.

## 2 Large- $x$ resummations

Large- $x$  resummations depend crucially on the kinematics and color structure of the process under study. In single-particle-inclusive (1PI) kinematics we identify one particle  $F$  with momentum  $p$ . In pair-invariant-mass (PIM) kinematics we identify a pair of particles (such as a heavy quark-antiquark pair) with invariant mass squared  $Q^2$ .

In general, the partonic cross section  $\hat{\sigma}$  includes soft corrections in the form of plus distributions  $\mathcal{D}_l(x_{th})$  with respect to a kinematical variable  $x_{th}$  that measures distance from threshold, with  $l \leq 2n - 1$  at  $n$ -th order in  $\alpha_s$  beyond the leading order. In 1PI kinematics,  $x_{th}$  is usually denoted as  $s_4$  (or  $s_2$ ) and is defined by  $s_4 = s + t + u - \sum m^2$ , where the sum is over the squared masses of all particles in the process. At threshold,  $s_4 = 0$ . The plus distributions are then of the form

$$\mathcal{D}_l(s_4) \equiv \left[ \frac{\ln^l(s_4/M^2)}{s_4} \right]_+, \quad (3)$$

where  $M$  is a hard scale relevant to the process, for example the mass  $m$  of a heavy quark or the transverse momentum of a jet. The plus distributions are defined through their integral with the parton distribution functions by

$$\begin{aligned} \int_0^{s_4^{max}} ds_4 \phi(s_4) \left[ \frac{\ln^l(s_4/M^2)}{s_4} \right]_+ &\equiv \int_0^{s_4^{max}} ds_4 \frac{\ln^l(s_4/M^2)}{s_4} [\phi(s_4) - \phi(0)] \\ &+ \frac{1}{l+1} \ln^{l+1} \left( \frac{s_4^{max}}{M^2} \right) \phi(0). \end{aligned} \quad (4)$$

In PIM kinematics,  $x_{th}$  is usually denoted as  $1 - x$  or  $1 - z$ , with  $z = Q^2/s \rightarrow 1$  at threshold. Then the plus distributions are of the form

$$\mathcal{D}_l(z) \equiv \left[ \frac{\ln^l(1-z)}{1-z} \right]_+ \quad (5)$$

defined by

$$\begin{aligned} \int_{z_{min}}^1 dz \phi(z) \left[ \frac{\ln^l(1-z)}{1-z} \right]_+ &\equiv \int_{z_{min}}^1 dz \frac{\ln^l(1-z)}{1-z} [\phi(z) - \phi(1)] \\ &+ \frac{1}{l+1} \ln^{l+1}(1-z_{min}) \phi(1). \end{aligned} \quad (6)$$

The highest powers of these distributions in the  $n$ th-order corrections are the leading logarithms (LL) with  $l = 2n - 1$ , the second highest are the next-to-leading logarithms (NLL) with  $l = 2n - 2$ , etc. (note that the counting of logarithms is different in the exponent and in the fixed-order expansions). These logarithms can be resummed in principle to all orders in perturbation theory.

## 2.1 Exponentiation

The resummation of threshold logarithms is performed in moment space. By taking moments, divergent distributions in  $1 - z$  (or  $s_4$ ) produce powers of  $\ln N$ , with  $N$  the moment variable:

$$\int_0^1 dz z^{N-1} \left[ \frac{\ln^m(1-z)}{1-z} \right]_+ = \frac{(-1)^{m+1}}{m+1} \ln^{m+1} N + \mathcal{O}(\ln^{m-1} N). \quad (7)$$

If we define moments of the partonic cross section by  $\hat{\sigma}(N) = \int dz z^{N-1} \hat{\sigma}(z)$  (PIM) or by  $\hat{\sigma}(N) = \int (ds_4/s) e^{-Ns_4/s} \hat{\sigma}(s_4)$  (1PI), then the logarithms of  $N$  that appear in  $\hat{\sigma}(N)$  exponentiate.

The resummation follows from the factorization properties of the cross section. We begin the derivation of the resummed cross section by first writing a factorized form for the moment-space infrared-regularized parton-parton scattering cross section,  $\sigma_{f_1 f_2 \rightarrow F}(N, \epsilon)$ , which factorizes as the hadronic cross section

$$\sigma_{f_1 f_2 \rightarrow F}(N, \epsilon) = \tilde{\phi}_{f_1/f_1}(N, \mu_F, \epsilon) \tilde{\phi}_{f_2/f_2}(N, \mu_F, \epsilon) \hat{\sigma}_{f_1 f_2 \rightarrow F}(N, \mu_F, \mu_R), \quad (8)$$

with the moments of  $\phi$  given by  $\tilde{\phi}(N) = \int_0^1 dx x^{N-1} \phi(x)$ . We factorize the initial-state collinear divergences, regularized by  $\epsilon$ , into the parton distribution functions,  $\phi$ , which are expanded to the same order in  $\alpha_s$  as the partonic cross section, and we thus obtain the perturbative expansion for the infrared-safe partonic short-distance function  $\hat{\sigma}$ .

The partonic short-distance function  $\hat{\sigma}$  still has sensitivity to soft-gluon dynamics through its  $N$  dependence. We then refactorize the moments of the cross section as [4, 8]

$$\sigma_{f_1 f_2 \rightarrow F}(N, \epsilon) = \tilde{\psi}_{f_1/f_1}(N, \mu_F, \epsilon) \tilde{\psi}_{f_2/f_2}(N, \mu_F, \epsilon) \times H_{IL}^{f_1 f_2 \rightarrow F}(\alpha_s(\mu_R)) \tilde{S}_{LI}^{f_1 f_2 \rightarrow F}\left(\frac{M}{N\mu_F}, \alpha_s(\mu_R)\right) \prod_j \tilde{J}_j(N, \mu_F, \epsilon) + \mathcal{O}(1/N), \quad (9)$$

where  $\psi$  are center-of-mass distributions that absorb the universal collinear singularities from the incoming partons,  $H_{IL}$  are  $N$ -independent hard components which describe the hard-scattering,  $S_{LI}$  is a soft gluon function associated with non-collinear soft gluons, and  $J$  are functions that absorb the collinear singularities from massless partons, if any, in the final state.

$H$  and  $S$  are matrices in color space and we sum over the color indices  $I$  and  $L$  that describe the color structure of the hard scattering. The hard-scattering function involves contributions from the amplitude of the process and the complex conjugate of the amplitude,

$H_{IL} = h_L^* h_I$ . The soft function  $S_{LI}$  represents the coupling of soft gluons to the partons in the scattering. The color tensors of the hard scattering connect together the eikonal lines to which soft gluons couple. One can construct an eikonal operator describing soft-gluon emission and write a dimensionless eikonal cross section, which describes the emission of soft gluons by the eikonal lines [4, 6–8].

Comparing Eqs. (8) and (9), we see that the moments of the short-distance partonic cross section are given by

$$\begin{aligned} \hat{\sigma}_{f_1 f_2 \rightarrow F}(N, \mu_F, \mu_R) &= \frac{\tilde{\psi}_{f_1/f_1}(N, \mu_F, \epsilon) \tilde{\psi}_{f_2/f_2}(N, \mu_F, \epsilon)}{\tilde{\phi}_{f_1/f_1}(N, \mu_F, \epsilon) \tilde{\phi}_{f_2/f_2}(N, \mu_F, \epsilon)} H_{IL}^{f_1 f_2 \rightarrow F}(\alpha_s(\mu_R)) \\ &\times \tilde{S}_{LI}^{f_1 f_2 \rightarrow F}\left(\frac{M}{N\mu_F}, \alpha_s(\mu_R)\right) \prod_j \tilde{J}_j(N, \mu_F, \epsilon). \end{aligned} \quad (10)$$

All the factors in Eq. (10) are gauge and factorization scale dependent. The constraint that the product of these factors must be independent of the gauge and factorization scale results in the exponentiation of logarithms of  $N$  in  $\psi/\phi$  and  $S_{LI}$  [4, 5].

The soft matrix  $S_{LI}$  depends on  $N$  through the ratio  $M/(N\mu_F)$ , and it requires renormalization as a composite operator. Its  $N$ -dependence can thus be resummed by renormalization group analysis [17–20]. However, the product  $H_{IL} S_{LI}$  needs no overall renormalization, because the UV divergences of  $S_{LI}$  are balanced by those of  $H_{IL}$ . Thus, we have [4, 8]

$$\begin{aligned} H_{IL}^0 &= \prod_{i=a,b} Z_i^{-1} \left( Z_S^{-1} \right)_{IC} H_{CD} \left[ \left( Z_S^\dagger \right)^{-1} \right]_{DL}, \\ S_{LI}^0 &= \left( Z_S^\dagger \right)_{LB} S_{BA} Z_{S,AI}, \end{aligned} \quad (11)$$

where  $H^0$  and  $S^0$  denote the unrenormalized quantities,  $Z_i$  is the renormalization constant of the  $i$ th incoming partonic field, and  $Z_S$  is a matrix of renormalization constants, which describe the renormalization of the soft function.  $Z_S$  is defined to include the wave function renormalization necessary for the outgoing eikonal lines that represent any heavy quarks.

From Eq. (11), we see that the soft function  $S_{LI}$  satisfies the renormalization group equation [4, 6–8]

$$\left( \mu \frac{\partial}{\partial \mu} + \beta(g_s) \frac{\partial}{\partial g_s} \right) S_{LI} = -(\Gamma_S^\dagger)_{LB} S_{BI} - S_{LA} (\Gamma_S)_{AI}, \quad (12)$$

where  $\beta$  is the QCD beta function and  $g_s^2 = 4\pi\alpha_s$ .  $\Gamma_S$  is an anomalous dimension matrix that is calculated in the eikonal approximation by explicit renormalization of the soft function. In a minimal subtraction renormalization scheme and with  $\epsilon = 4 - n$ , where  $n$  is the number of space-time dimensions, the soft anomalous dimension matrix is given at one loop by

$$\Gamma_S^{(1l)}(g_s) = -\frac{g_s}{2} \frac{\partial}{\partial g_s} \text{Res}_{\epsilon \rightarrow 0} Z_S(g_s, \epsilon). \quad (13)$$

The process-dependent matrices  $\Gamma_S$  have been calculated at one loop for all  $2 \rightarrow 2$  partonic processes; a compilation of results is given in [8]. In processes with trivial or simple color structure  $\Gamma_S$  is simply a function ( $1 \times 1$  matrix) while in processes with complex color structure it is a non-trivial matrix in color exchange. For quark-(anti)quark scattering,  $\Gamma_S$  is a  $2 \times 2$  matrix [4, 18]; for quark-gluon scattering it is a  $3 \times 3$  matrix [7]; for gluon-gluon scattering it is an  $8 \times 8$  matrix [7]. Complete two-loop calculations of soft anomalous dimensions for processes with massless quarks have appeared in [21]. Selected two-loop results for heavy quark production appeared in [22]. We present a sample one-loop calculation in Section 4.1 and a sample two-loop calculation in Section 4.2, both with outgoing massive quarks (see [23]).

The exponentiation of logarithms of  $N$  in the ratios  $\psi/\phi$  and in the functions  $J$  in Eq. (10), together with the solution of the renormalization group equation (12), provide us with the complete expression for the resummed partonic cross section in moment space [4, 6–8, 24, 25]

$$\begin{aligned} \hat{\sigma}^{res}(N) &= \exp \left[ \sum_i E^{f_i}(N_i) \right] \exp \left[ \sum_j E'^{f_j}(N_j) \right] \\ &\times \exp \left[ \sum_i 2 \int_{\mu_F}^{\sqrt{s}} \frac{d\mu}{\mu} \gamma_{f_i/f_i}(\alpha_s(\mu)) \right] \exp \left[ 2 d_{\alpha_s} \int_{\mu_R}^{\sqrt{s}} \frac{d\mu}{\mu} \beta(\alpha_s(\mu)) \right] \\ &\times \text{Tr} \left\{ H^{f_1 f_2 \rightarrow F}(\alpha_s(\mu_R)) \exp \left[ \int_{\sqrt{s}}^{\sqrt{s}/\tilde{N}_j} \frac{d\mu}{\mu} \Gamma_S^{\dagger f_1 f_2 \rightarrow F}(\alpha_s(\mu)) \right] \right. \\ &\times \tilde{S}^{f_1 f_2 \rightarrow F} \left( \alpha_s \left( \frac{\sqrt{s}}{\tilde{N}_j} \right) \right) \exp \left[ \int_{\sqrt{s}}^{\sqrt{s}/\tilde{N}_j} \frac{d\mu}{\mu} \Gamma_S^{f_1 f_2 \rightarrow F}(\alpha_s(\mu)) \right] \left. \right\}. \quad (14) \end{aligned}$$

The sums over  $i = 1, 2$  run over incoming partons. The sum over  $j$  is over massless partons, if any, in the final state at lowest order. The resummed expression is valid for either 1PI or PIM kinematics. In 1PI kinematics  $N_i = N(-t_i/M^2)$ , where  $t_i$  denotes  $t$  or  $u$ , and  $N_j = N(s/M^2)$ , while in PIM kinematics  $N_i = N_j = N$ . Also  $\tilde{N} = N e^{\gamma_E}$ , with  $\gamma_E$  the Euler constant.

The first exponent in Eq. (14) arises from the exponentiation of logarithms of  $N$  in the ratios  $\psi/\phi$  of Eq. (10), and is given in the  $\overline{\text{MS}}$  scheme by

$$E^{f_i}(N_i) = - \int_0^1 dz \frac{z^{N_i-1} - 1}{1-z} \left\{ \int_{(1-z)^2}^1 \frac{d\lambda}{\lambda} A_i(\alpha_s(\lambda s)) + \nu_i [\alpha_s((1-z)^2 s)] \right\}, \quad (15)$$

with  $A_i(\alpha_s) = \sum_{n=1}^{\infty} (\alpha_s/\pi)^n A_i^{(n)}$ . At one loop,  $A_i^{(1)} = C_i$  which is  $C_F = (N_c^2 - 1)/(2N_c)$  for a quark or antiquark and  $C_A = N_c$  for a gluon, with  $N_c$  the number of colors, while  $A_i^{(2)} = C_i K/2$  with  $K = C_A(67/18 - \zeta_2) - 5n_f/9$  [26], where  $n_f$  is the number of quark flavors and  $\zeta_2 = \pi^2/6$ . Also  $\nu_i = \sum_{n=1}^{\infty} (\alpha_s/\pi)^n \nu_i^{(n)}$ , with  $\nu_i^{(1)} = C_i$ .

The second exponent in Eq. (14) arises from the exponentiation of logarithms of  $N$  in

the functions  $J_j$  of Eq. (10), and is given by

$$E'^{f_j}(N_j) = \int_0^1 dz \frac{z^{N_j-1} - 1}{1-z} \left\{ \int_{(1-z)^2}^{1-z} \frac{d\lambda}{\lambda} A_j(\alpha_s(\lambda s)) - B_j[\alpha_s((1-z)s)] - \nu_j [\alpha_s((1-z)^2 s)] \right\}. \quad (16)$$

Here  $B_j = \sum_{n=1}^{\infty} (\alpha_s/\pi)^n B_j^{(n)}$  with  $B_j^{(1)}$  equal to  $3C_F/4$  for quarks and  $\beta_0/4$  for gluons, where  $\beta_0 = (11C_A - 2n_f)/3$  is the lowest-order  $\beta$  function.

The third exponent in Eq. (14) controls the factorization scale dependence of the cross section, and  $\gamma_{f_i/f_i}$  is the moment-space anomalous dimension of the  $\overline{\text{MS}}$  density  $\phi_{f_i/f_i}$ . The  $\beta$  function in the fourth exponent controls the renormalization scale dependence of the cross section. The constant  $d_{\alpha_s}$  takes the value  $k$  if the Born cross section is of order  $\alpha_s^k$ . Explicit expressions for the functions in these four exponents, and related references, are assembled for convenience in Appendix A of Ref. [27].

As noted before, both  $H$  and  $S$  are process-dependent matrices in color space and thus the trace is taken in Eq. (14). At lowest order, the trace of the product of  $H$  and  $S$  reproduces the Born cross section. The evolution of the soft function  $S$  follows from its renormalization group equation, (12), and is given in terms of the soft anomalous dimension matrix  $\Gamma_S$ .

## 2.2 NNNLO expansions

The exponentials in the resummed partonic cross section can be expanded to any fixed order in  $\alpha_s$  and then inverted to momentum space to provide explicit results for the higher-order corrections. A fixed-order expansion avoids using a prescription to regulate the infrared singularities in the exponents and thus no prescription is needed to deal with these in this approach (see discussion in Ref. [28]).

We now expand the resummed cross section, Eq. (14), in 1PI kinematics through NNNLO. We provide results here for the case where  $\Gamma_S$  are trivial ( $1 \times 1$ ) color matrices. Explicit expressions for the more general case are found through NNLO in [24] and through NNNLO in [25].

At NLO, we find the expression for the soft-gluon corrections

$$\hat{\sigma}^{(1)} = \sigma^B \frac{\alpha_s(\mu_R^2)}{\pi} \{c_3 \mathcal{D}_1(s_4) + c_2 \mathcal{D}_0(s_4) + c_1 \delta(s_4)\} \quad (17)$$

where  $\sigma^B$  is the leading-order (LO) term, the LL coefficient is

$$c_3 = \sum_i 2C_i - \sum_j C_j, \quad (18)$$

with  $C_q = C_F$  and  $C_g = C_A$ , and the NLL coefficient  $c_2$  is defined by  $c_2 = c_2^\mu + T_2$ , with

$$c_2^\mu = - \sum_i C_i \ln \left( \frac{\mu_F^2}{M^2} \right) \quad (19)$$

denoting the terms involving logarithms of the factorization scale, and

$$T_2 = 2\text{Re}\Gamma_S^{(1)} - \sum_i \left[ C_i + 2 C_i \ln \left( \frac{-t_i}{M^2} \right) + C_i \ln \left( \frac{M^2}{s} \right) \right] - \sum_j \left[ B_j^{(1)} + C_j + C_j \ln \left( \frac{M^2}{s} \right) \right] \quad (20)$$

denoting the scale-independent terms. Again,  $t_i$  denotes  $t$  or  $u$ , the sums over  $i$  run over incoming partons, and the sums over  $j$  run over any massless partons in the final state at LO.

We write the NLO  $\delta(s_4)$  terms as  $c_1 = c_1^\mu + T_1$ , where

$$c_1^\mu = \sum_i \left[ C_i \ln \left( \frac{-t_i}{M^2} \right) - \gamma_i^{(1)} \right] \ln \left( \frac{\mu_F^2}{M^2} \right) + d_{\alpha_s} \frac{\beta_0}{4} \ln \left( \frac{\mu_R^2}{M^2} \right) \quad (21)$$

denotes the terms involving logarithms of the factorization and renormalization scales. Here  $\gamma_q^{(1)} = 3C_F/4$  and  $\gamma_g^{(1)} = \beta_0/4$ , and  $T_1$  denotes virtual terms that cannot be derived from the resummation formalism but can be determined by matching to a full NLO calculation for any specified process.

At NNLO, the soft-gluon corrections are

$$\begin{aligned} \hat{\sigma}^{(2)} = & \sigma^B \frac{\alpha_s^2(\mu_R^2)}{\pi^2} \left\{ \frac{1}{2} c_3^2 \mathcal{D}_3(s_4) + \left[ \frac{3}{2} c_3 c_2 - \frac{\beta_0}{4} c_3 + \sum_j C_j \frac{\beta_0}{8} \right] \mathcal{D}_2(s_4) \right. \\ & + \left[ c_3 c_1 + c_2^2 - \zeta_2 c_3^2 - \frac{\beta_0}{2} T_2 + \frac{\beta_0}{4} c_3 \ln \left( \frac{\mu_R^2}{M^2} \right) + c_3 \frac{K}{2} - \sum_j \frac{\beta_0}{4} B_j^{(1)} \right] \mathcal{D}_1(s_4) \Big\} \\ & + \dots \end{aligned} \quad (22)$$

where we show explicitly results through next-to-next-to-leading logarithms (NNLL). For a complete expression see [24, 25].

At NNNLO, the soft-gluon corrections are

$$\begin{aligned} \hat{\sigma}^{(3)} = & \sigma^B \frac{\alpha_s^3(\mu_R^2)}{\pi^3} \left\{ \frac{1}{8} c_3^3 \mathcal{D}_5(s_4) + \left[ \frac{5}{8} c_3^2 c_2 - \frac{5}{24} \beta_0 c_3^2 + \frac{5}{48} c_3 \beta_0 \sum_j C_j \right] \mathcal{D}_4(s_4) \right. \\ & + \left[ c_3 c_2^2 + \frac{1}{2} c_3^2 c_1 - \zeta_2 c_3^3 + \frac{\beta_0^2}{12} c_3 - \frac{\beta_0}{3} c_3 c_2 - \frac{\beta_0}{2} c_3 T_2 + \frac{\beta_0}{4} c_3^2 \ln \left( \frac{\mu_R^2}{M^2} \right) \right. \\ & \left. \left. + c_3^2 \frac{K}{2} + c_2 \frac{\beta_0}{6} \sum_j C_j - c_3 \sum_j \frac{\beta_0}{4} B_j^{(1)} - \sum_j C_j \frac{3\beta_0^2}{48} \right] \mathcal{D}_3(s_4) \right\} + \dots \end{aligned} \quad (23)$$

where again we show explicitly results through NNLL. The complete expression is given in [25].



In PIM kinematics we simply replace  $s_4$  by  $1 - z$ , set  $s = M^2$ , and drop the terms with  $\ln(-t_i/M^2)$  in the above formulas.

The NNNLO master equation, (23), gives the structure of the soft corrections and can provide the full soft corrections explicitly if all the necessary two-loop and three-loop quantities are known. For processes with non-trivial color structure we are currently limited to NLL or NNLL accuracy. For processes with trivial color structure, such as  $b\bar{b} \rightarrow H$  [27, 29], all soft-gluon corrections have been determined through NNNLO. Below, the term “ $N^{(n)}\text{LO-}N^{(l)}\text{LL}$ ” means that the soft-gluon contributions through  $N^{(l)}\text{LL}$  accuracy to the  $n$ -th order QCD corrections have been included.

### 3 Applications of large- $x$ resummations

In this section we provide some calculations that are applications of the large- $x$  resummation formalism to processes of interest at the Tevatron and the LHC. We present results for top-antitop pair production, single top quark production,  $W$ -boson production, and Higgs boson production via  $b\bar{b} \rightarrow H$ .

#### 3.1 $t\bar{t}$ production

The top quark, the heaviest known elementary particle, was discovered in  $p\bar{p}$  collisions at Run I of the Tevatron in 1995 [30, 31]. More recent measurements at Run II have increased the accuracy of the top mass and cross section measurements (for a review see [32, 33]) and thus require accurate theoretical calculations of top production cross sections and differential distributions. The main partonic channels in  $t\bar{t}$  production are  $q\bar{q} \rightarrow t\bar{t}$ , which is dominant at the Tevatron, and  $gg \rightarrow t\bar{t}$ , which will be dominant at the LHC.

The latest calculation for top-antitop pair hadroproduction includes NNLO soft-gluon corrections to the double differential cross section [34]. Near threshold the soft-gluon corrections dominate the cross section at the Tevatron and contribute sizable enhancements. The form of the corrections and their numerical values depend crucially on the kinematics chosen to describe the process. The NNLO soft corrections were calculated fully to NNLL in both IPI and PIM kinematics [28, 35]. In addition a good approximation for the next-to-next-to-next-to-leading logarithms (NNNLL) was provided in [34]. The best theoretical result for the cross section is the average of the NNLO-NNNLL cross sections in the two different kinematics [34].

In Fig. 1, we present the NLO and approximate NNLO-NNNLL  $t\bar{t}$  cross sections at the Tevatron with  $\sqrt{S} = 1.96$  TeV using the MRST2002 [36] parton densities. On the left we plot the cross sections as functions of  $m_t$ , the top quark mass, for  $\mu = m_t$ , where  $\mu$  denotes the factorization and renormalization scales which we have set equal to each other. On the right we plot the cross sections as functions of  $\mu/m_t$  with  $m_t = 175$  GeV. The results are given in both IPI and PIM kinematics together with their average. The NLO cross section depends less on  $\mu$  than the LO cross section, as expected. The NNLO-NNNLL cross sections exhibit even less dependence on  $\mu$ , approaching the scale independence of a true

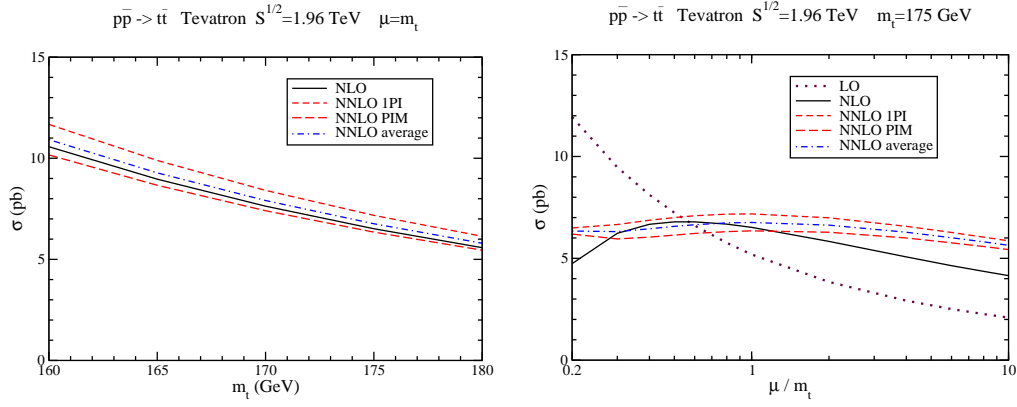


Figure 1: The  $t\bar{t}$  total cross sections in  $p\bar{p}$  collisions at the Tevatron with  $\sqrt{S} = 1.96$  TeV as functions of  $m_t$  (left) and  $\mu/m_t$  (right).

physical cross section. They change by less than 3% in the range  $m_t/2 < \mu < 2m_t$ . For a top mass of 175 GeV the average of the NNLO-NNLL 1PI and PIM results is  $6.77 \pm 0.42$  pb, where the uncertainty indicated is from the kinematics. Including all sources of uncertainty (kinematics, scale variation, and uncertainty from the parton distribution functions) we may write the cross section as  $6.8 \pm 0.6$  pb. This theoretical result is in agreement with the latest experimental result for the cross section at the Tevatron [37, 38]. Finally, we note that NNNLO soft-gluon contributions in the  $q\bar{q} \rightarrow t\bar{t}$  channel were presented in [25]. These NNNLO-NNLL corrections further stabilize the scale dependence of the cross section at the Tevatron.

### 3.2 Single top quark production

Single top quark production provides a way to directly measure electroweak properties of the top quark, such as the  $V_{tb}$  CKM matrix element. It also allows a deeper study of electroweak theory since the top quark mass is of the same order of magnitude as the electroweak symmetry breaking scale, and may be useful in the discovery of new physics. Therefore it is crucial to have accurate theoretical predictions for the cross section.

The cross section for single top quark production is less than the  $t\bar{t}$  cross section and the backgrounds to the production processes make the extraction of the single top signal challenging. Intensive searches for single top quark events at the Tevatron have recently produced evidence of such events [39, 40]. The LHC has good potential for observation and further analysis of single top events.

Single top quarks can be produced through three distinct partonic processes. One is  $t$ -channel production,  $qb \rightarrow q't$  and  $\bar{q}b \rightarrow \bar{q}'t$ , via the exchange of a space-like  $W$  boson, a second is  $s$ -channel production,  $q\bar{q}' \rightarrow \bar{b}t$ , via the exchange of a time-like  $W$  boson, and a third is associated  $tW$  production,  $bg \rightarrow tW^-$ .

The threshold corrections to single top production have been calculated for both the

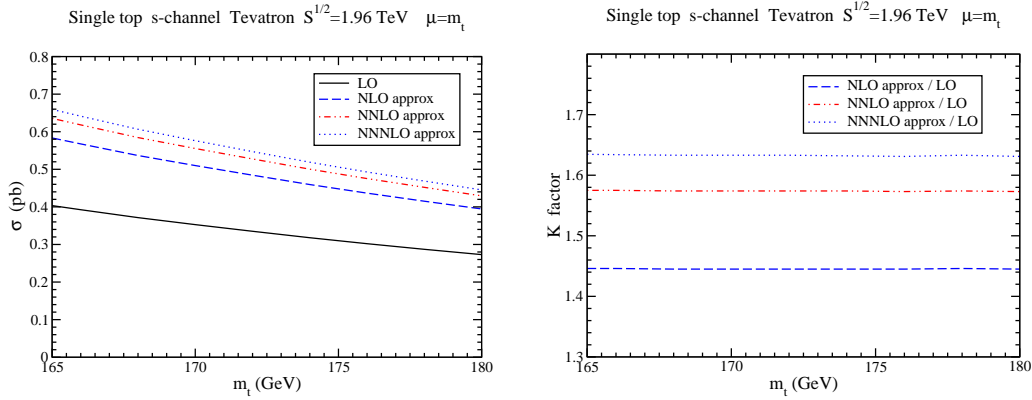


Figure 2: The cross section (left) and  $K$  factors (right) for single top quark production at the Tevatron in the  $s$  channel. Here  $\mu = \mu_F = \mu_R = m_t$ .

Tevatron and LHC colliders through NNNLO [41–43]. At the Tevatron the  $t$ -channel process is numerically dominant, but the higher-order corrections are relatively small. The  $s$ -channel is smaller, but receives large corrections and it was shown that the threshold soft-gluon corrections dominate the cross section. Associated  $tW$  production is quite minor, although it also has large  $K$  factors, defined as the ratios of the higher-order cross sections to the LO cross section. At the LHC the  $t$  channel is again dominant, but the second largest channel is  $tW$  production; the  $s$  channel is numerically the smallest. Below we provide some numerical results for all three channels at both the Tevatron and the LHC colliders using the MRST2004 parton densities [44]. We add the soft-gluon corrections through NNNLO to the complete NLO cross section [45, 46].

We begin with single top production at the Tevatron [41] with  $\sqrt{S} = 1.96$  TeV. For  $t$ -channel production, the NNNLO-NLL cross section is  $\sigma^{t\text{-channel}}(m_t = 175 \text{ GeV}) = 1.08^{+0.02}_{-0.01} \pm 0.06$  pb, where the first uncertainty is from variation of the factorization and renormalization scales,  $\mu_F$  and  $\mu_R$ , between  $m_t/2$  and  $2m_t$ , and the second is due to the parton distribution functions. For the  $s$  channel, the corresponding cross section is  $\sigma^{s\text{-channel}}(m_t = 175 \text{ GeV}) = 0.49 \pm 0.02 \pm 0.01$  pb. Finally, in the  $tW$  channel  $\sigma^{tW}(m_t = 175 \text{ GeV}) = 0.13 \pm 0.02 \pm 0.02$  pb. We note that the cross sections for antitop production at the Tevatron are identical to those for single top production in each channel.

In Fig. 2 we plot the cross section and the  $K$  factors for single top quark production at the Tevatron in the  $s$  channel setting both the factorization and renormalization scales to  $\mu = m_t$ . We plot the LO cross section and the approximate NLO, NNLO, and NNNLO cross sections at NLL accuracy. The  $K$  factors are quite large, thus showing that the corrections provide a big enhancement to the cross section.

We continue with single top production at the LHC [42] with  $\sqrt{S} = 14$  TeV. For the  $t$  channel the threshold corrections are not a good approximation of the complete corrections. The NLO cross section for top production  $\sigma_{\text{top}}^{t\text{-channel}}(m_t = 175 \text{ GeV}) = 146 \pm 4 \pm 3$  pb. For antitop production the corresponding result is  $\sigma_{\text{antitop}}^{t\text{-channel}}(m_t =$

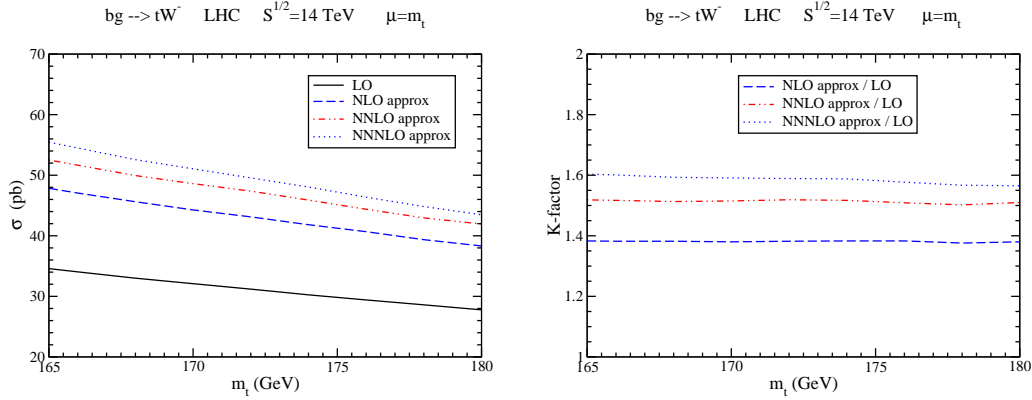


Figure 3: The cross section (left) and  $K$  factors (right) for associated  $tW$  production at the LHC. Here  $\mu = \mu_F = \mu_R = m_t$ .

175 GeV) =  $89 \pm 3 \pm 2$  pb. For the  $s$  channel, the soft-gluon corrections are relatively large and the soft-gluon approximation is good. The NNNLO-NLL cross section is  $\sigma_{\text{top}}^{s\text{-channel}}(m_t = 175 \text{ GeV}) = 7.23^{+0.53}_{-0.45} \pm 0.13$  pb for single top production and  $\sigma_{\text{antitop}}^{s\text{-channel}}(m_t = 175 \text{ GeV}) = 4.03^{+0.10}_{-0.12} \pm 0.10$  pb for single antitop production. Finally, for  $tW$  production the cross section is  $\sigma^{tW}(m_t = 175 \text{ GeV}) = 41.1 \pm 4.1 \pm 1.0$  pb, which is identical to that for associated antitop production. In Fig. 3 we plot the cross section and  $K$  factors for associated  $tW$  production at the LHC setting the scales to  $\mu = m_t$ . As seen from the plots, the soft-gluon corrections are large for this process.

### 3.3 $W$ -boson production at large transverse momentum

$W$ -boson production in hadron colliders can be used in testing the Standard Model and in estimating backgrounds to Higgs production and new physics. Precise calculations for  $W$  production at large transverse momentum,  $Q_T$ , are needed to identify signals of new physics which may be expected to enhance the  $Q_T$  distribution at high  $Q_T$ .

Analytical NLO calculations of the cross section for  $W$  production at large transverse momentum were presented in Refs. [47, 48], where numerical results were also presented for the Fermilab Tevatron. Numerical NLO results for  $W$  production at the LHC were more recently presented in [49]. The NLO corrections enhance the  $Q_T$  distribution of the  $W$  boson and they reduce the factorization and renormalization scale dependence of the cross section.

A recent theoretical study [50] included soft-gluon corrections through NNLO, which provide additional enhancements and a further reduction of the scale dependence. The complete NNLL terms were calculated and an approximation for the NNNLL terms was derived at NNLO. Numerical results with these soft corrections were calculated for  $W$  production at the Tevatron [50] and the LHC [49].

Here we discuss  $W$  production at large transverse momentum at the LHC with  $\sqrt{S} = 14$

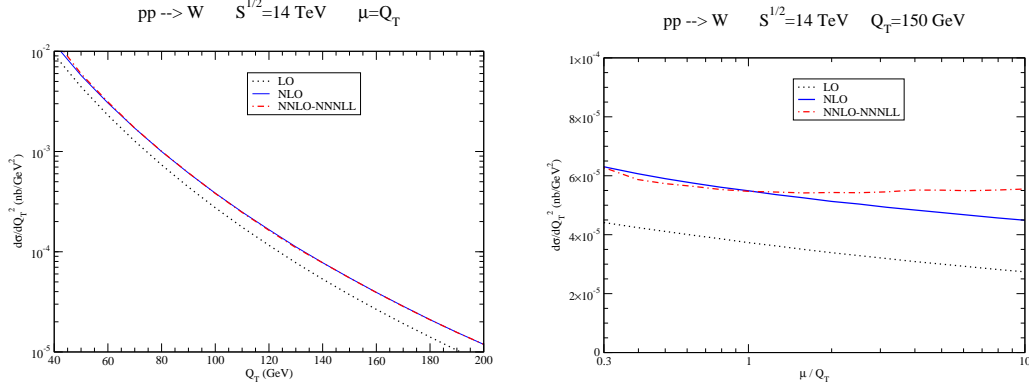


Figure 4: The differential cross section,  $d\sigma/dQ_T^2$ , for  $W$  production at the LHC with  $\mu = Q_T$  (left) and  $Q_T = 150$  GeV (right).

TeV using the MRST2002 parton densities [36]. The LO partonic processes for the production of a  $W$  boson and a parton are  $qg \rightarrow Wq$  and  $q\bar{q} \rightarrow Wg$ . The electroweak coupling  $\alpha(M_Z^2)$  is evaluated at the mass of the  $Z$  boson, and standard values [51] are used for the various electroweak parameters. In the numerical results we present the sum of cross sections for  $W^-$  and  $W^+$  production. The  $W$  bosons at the LHC will be detected primarily through their leptonic decay products e.g.,  $W^- \rightarrow \ell\bar{\nu}_\ell$ , therefore the cross sections presented here should be multiplied by the appropriate branching ratios.

In Fig. 4 (left plot) we plot the transverse momentum distribution,  $d\sigma/dQ_T^2$ , at high  $Q_T$  for  $W$  production at the LHC. We set  $\mu_F = \mu_R = Q_T$  and denote this common scale by  $\mu$ . We plot LO, NLO, and NNLO-NNLL results using the corresponding parton densities. As seen from the plot, the NLO corrections provide a significant enhancement of the LO  $Q_T$  distribution. The NNLO-NNLL corrections provide a rather small further enhancement of the  $Q_T$  distribution. However, the NNLO-NNLL corrections can be much bigger for other choices of factorization and renormalization scales. The NLO corrections increase the LO result by about 30% to 50% in the  $Q_T$  range shown. In contrast, the NNLO-NNLL/NLO ratio for this scale is rather small. Part of the reason for this is that the NNLO parton distribution functions are significantly smaller than the NLO pdf.

On the plot on the right in Fig. 4 we show the scale dependence of  $d\sigma/dQ_T^2$  for  $Q_T = 150$  GeV versus  $\mu/Q_T$  over two orders of magnitude. It is interesting to note that the scale dependence of the cross section is not reduced when the NLO corrections are included. This is due to the fact that the cross section is dominated by the process  $qg \rightarrow Wq$ . The gluon density in the proton, at fixed  $x$  less than  $\sim 0.01$ , increases rapidly with scale. Thus, the  $\mu_R$  and  $\mu_F$  dependencies cancel one another to a large extent. However, we have an improvement in the scale variation when the NNLO-NNLL corrections are added. The NNLO-NNLL result displays very little scale dependence.

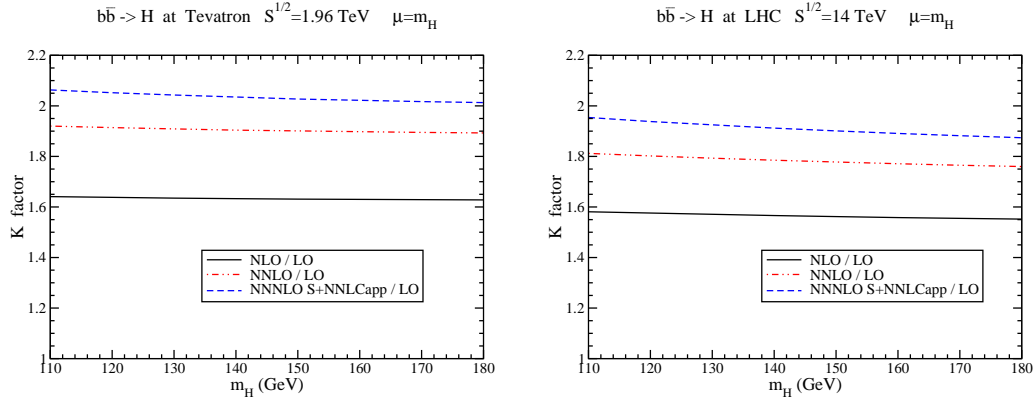


Figure 5: The  $K$  factors for  $b\bar{b} \rightarrow H$  at the Tevatron (left) and the LHC (right). Here  $\mu = \mu_F = \mu_R = m_H$ .

### 3.4 Higgs boson production via $b\bar{b} \rightarrow H$

The search for the Higgs boson [52] is one of the most important goals at the Tevatron and the LHC colliders [53]. The main Standard Model production channel at these colliders is  $gg \rightarrow H$ . However, the channel  $b\bar{b} \rightarrow H$  can be competitive in the Minimal Supersymmetric Standard Model at high  $\tan \beta$ , with  $\tan \beta$  the ratio of the vacuum expectation values for the two Higgs doublets. The complete NNLO QCD corrections for this process were calculated in [54].

Complete expressions for the soft-gluon corrections at NNNLO were presented in [27, 29]. However, it is known at NNLO that the soft corrections alone are not a good approximation of the full corrections [27, 54]. Purely collinear terms [27, 55, 56] have to be included to provide an accurate calculation. An approximation for the collinear terms through NNLL accuracy at NNNLO was provided in [27].

We now present numerical results for  $b\bar{b} \rightarrow H$  at the Tevatron and the LHC [27] using the MRST2006 parton densities [57]. Figure 5 shows the  $K$  factors for Higgs production via  $b\bar{b} \rightarrow H$  at the Tevatron (left) and the LHC (right), with  $\mu = m_H$ . The complete NLO corrections increase the LO result by around 60% at both the Tevatron and the LHC. Inclusion of the complete NNLO corrections further increases the cross section: the NNLO  $K$  factor is around 1.9 at the Tevatron and 1.8 at the LHC. By including at NNNLO the sum of the complete soft-gluon corrections and the collinear approximate NNLL corrections (S+NNLLapp), we find further enhancement. From the study of the contributions of the soft and collinear terms at NLO and NNLO at both the Tevatron and the LHC we expect that the NNNLO S+NNLCapp curve provides a good approximation of the complete NNNLO cross section. The NNNLO S+NNLCapp  $K$  factor is between 2.06 and 2.01 at the Tevatron and between 1.95 and 1.87 at the LHC for Higgs masses ranging between 110 and 180 GeV, which is a significant addition to the NNLO result.

## 4 Loop calculations in the eikonal approximation

The soft-gluon resummation formalism, and in particular the calculation of the soft anomalous dimension matrices, employs the use of the eikonal approximation in loop diagrams. The eikonal approximation is valid for describing the emission of soft gluons from partons in the hard scattering. The approximation leads to a simplified form of the Feynman rules by removing the Dirac matrices from the calculation. When the gluon momentum goes to zero, the Feynman rules for the quark propagator and quark-gluon vertex in Figure 6 simplify as follows:

$$\bar{u}(p) (-ig_s T_F^c) \gamma^\mu \frac{i(\not{p} + \not{k} + m)}{(p+k)^2 - m^2 + i\epsilon} \rightarrow \bar{u}(p) g_s T_F^c \gamma^\mu \frac{\not{p} + m}{2p \cdot k + i\epsilon} = \bar{u}(p) g_s T_F^c \frac{v^\mu}{v \cdot k + i\epsilon} \quad (24)$$

with  $v$  a dimensionless vector,  $p \propto v$ , and  $T_F^c$  the generators of SU(3) in the fundamental representation.

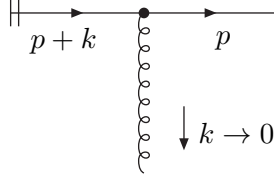


Figure 6: Eikonal approximation.

The ultraviolet poles in loop diagrams involving eikonal lines are particularly important as they play a direct role in the renormalization group evolution equations that are used in threshold resummations [4, 6, 7] (see Eq. (13)).

Below we give examples of a one-loop and a two-loop calculation for diagrams involving eikonal lines representing massive quarks. For the calculation we use the Feynman gauge, and we use dimensional regularization with  $n = 4 - \epsilon$  dimensions.

### 4.1 One-loop calculation

In this subsection we calculate the integral  $I_{1l}$  for the one-loop diagram in Fig. (7) with eikonal lines representing outgoing massive quarks. This one-loop integral is given by

$$I_{1l} = g_s^2 \int \frac{d^n k}{(2\pi)^n} \frac{(-i)g_{\mu\nu}}{k^2} \frac{v_i^\mu}{v_i \cdot k} \frac{(-v_j^\nu)}{(-v_j \cdot k)}. \quad (25)$$

Using Feynman parameterization, this integral can be rewritten as

$$I_{1l} = -2ig_s^2 \frac{v_i \cdot v_j}{(2\pi)^n} \int_0^1 dx \int_0^{1-x} dy \int \frac{d^n k}{[xk^2 + yv_i \cdot k + (1-x-y)v_j \cdot k]^3}. \quad (26)$$

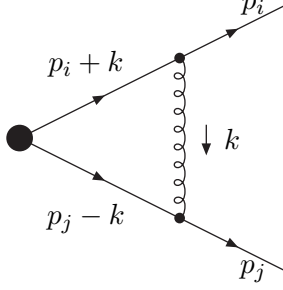


Figure 7: One-loop eikonal diagram with outgoing massive quarks.

After several manipulations, Eq. (26) becomes

$$I_{1l} = \frac{\alpha_s}{\pi} (-1)^{-1-\epsilon/2} 2^{5\epsilon/2} \pi^{\epsilon/2} \Gamma\left(1 + \frac{\epsilon}{2}\right) (1 + \beta^2) \int_0^1 dx x^{-1+\epsilon} (1-x)^{-1-\epsilon} \\ \times \left\{ \int_0^1 dz \left[ 4z\beta^2(1-z) + 1 - \beta^2 \right]^{-1} - \frac{\epsilon}{2} \int_0^1 dz \frac{\ln[4z\beta^2(1-z) + 1 - \beta^2]}{4z\beta^2(1-z) + 1 - \beta^2} + \mathcal{O}(\epsilon^2) \right\} \quad (27)$$

where here  $\beta = \sqrt{1 - 4m^2/s}$ , with  $m$  the quark mass, and we have used the relations  $v_i \cdot v_j = (1 + \beta^2)/2$  and  $v_i^2 = v_j^2 = (1 - \beta^2)/2$ .

The integral over  $x$  in Eq. (27) contains both ultraviolet (UV) and infrared (IR) singularities. We isolate the UV singularities and find that

$$\int_0^1 dx x^{-1+\epsilon} (1-x)^{-1-\epsilon} = \frac{1}{\epsilon} + \text{IR}. \quad (28)$$

After calculating the integrals over  $z$  in Eq. (27), we find that the UV poles and constant terms of  $I_{1l}$  are

$$I_{1l}^{UV} = \frac{\alpha_s}{\pi} \frac{(1 + \beta^2)}{2\beta} \left\{ \frac{1}{\epsilon} \ln\left(\frac{1 - \beta}{1 + \beta}\right) + \frac{1}{2} (4 \ln 2 + \ln \pi - \gamma_E - i\pi) \ln\left(\frac{1 - \beta}{1 + \beta}\right) \right. \\ \left. + \frac{1}{4} \ln^2(1 + \beta) - \frac{1}{4} \ln^2(1 - \beta) - \frac{1}{2} \text{Li}_2\left(\frac{1 + \beta}{2}\right) + \frac{1}{2} \text{Li}_2\left(\frac{1 - \beta}{2}\right) \right\}. \quad (29)$$

Complete one-loop calculations for heavy quark production in axial gauge were presented in Ref. [4].

## 4.2 Two-loop calculation

In this subsection we calculate the two-loop integral  $I_{2l}$  for the quark-loop diagram in Fig. (8) given by

$$I_{2l} = (-1) n_f g_s^4 \int \frac{d^n k}{(2\pi)^n} \frac{d^n l}{(2\pi)^n} \frac{v_i^\mu}{v_i \cdot k} \frac{(-v_j^\rho)}{(-v_j \cdot k)} \frac{(-i)g_{\mu\nu}}{k^2} \frac{(-i)g_{\rho\sigma}}{k^2}$$



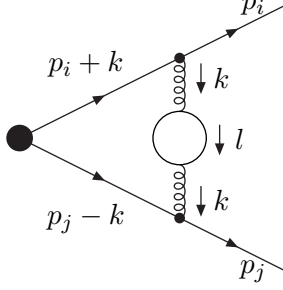


Figure 8: Two-loop eikonal diagram, involving a quark loop, with outgoing massive quarks.

$$\times \text{Tr} \left[ -i\gamma^\nu \frac{i\not{l}}{l^2} (-i)\gamma^\sigma i \frac{(\not{l} - \not{k})}{(l-k)^2} \right]. \quad (30)$$

After a few manipulations involving the trace we can write this integral as

$$I_{2l} = -4n_f \frac{g_s^4}{(2\pi)^{2n}} \left[ I_{2l}^a + I_{2l}^b + I_{2l}^c + I_{2l}^d + I_{2l}^e \right] \quad (31)$$

where

$$I_{2l}^a = v_i \cdot v_j \int \frac{d^n k}{v_i \cdot k v_j \cdot k k^4} \int \frac{d^n l}{(l-k)^2} \quad (32)$$

$$I_{2l}^b = -v_i \cdot v_j \int \frac{d^n k}{v_i \cdot k v_j \cdot k k^4} \int d^n l \frac{l \cdot k}{l^2 (l-k)^2} \quad (33)$$

$$I_{2l}^c = -2 \int \frac{d^n k}{v_i \cdot k v_j \cdot k k^4} \int d^n l \frac{v_i \cdot l v_j \cdot l}{l^2 (l-k)^2} \quad (34)$$

$$I_{2l}^d = \int \frac{d^n k}{v_i \cdot k k^4} \int d^n l \frac{v_i \cdot l}{l^2 (l-k)^2} \quad (35)$$

$$I_{2l}^e = \int \frac{d^n k}{v_j \cdot k k^4} \int d^n l \frac{v_j \cdot l}{l^2 (l-k)^2}. \quad (36)$$

We begin with the evaluation of  $I_{2l}^a$ . Since

$$\int \frac{d^n l}{(l-k)^2} = 0 \quad (37)$$

we find  $I_{2l}^a = 0$ .

Next we evaluate  $I_{2l}^b$ . Using Feynman parameterization, we find

$$\int d^n l \frac{l^\mu}{l^2 (l-k)^2} = i\pi^{(5-\epsilon)/2} 2^{-2+\epsilon} \Gamma\left(\frac{\epsilon}{2}\right) \frac{\Gamma(1-\frac{\epsilon}{2})}{\Gamma(\frac{3}{2}-\frac{\epsilon}{2})} (k^2)^{-\epsilon/2} k^\mu \quad (38)$$

therefore

$$I_{2l}^b = -i\pi^{(5-\epsilon)/2} 2^{-2+\epsilon} v_i \cdot v_j \Gamma\left(\frac{\epsilon}{2}\right) \frac{\Gamma\left(1-\frac{\epsilon}{2}\right)}{\Gamma\left(\frac{3}{2}-\frac{\epsilon}{2}\right)} \int \frac{d^n k}{v_i \cdot k v_j \cdot k (k^2)^{1+\epsilon/2}}. \quad (39)$$

The  $k$  integral in the above expression is

$$\begin{aligned} \int \frac{d^n k}{v_i \cdot k v_j \cdot k (k^2)^{1+\epsilon/2}} &= i\pi^{2-\epsilon/2} 2^{2+2\epsilon} (-1)^{-1-\epsilon} \frac{\Gamma(1+\epsilon)}{\Gamma\left(1+\frac{\epsilon}{2}\right)} \\ &\times \int_0^1 dx x^{-1+2\epsilon} (1-x)^{-1-2\epsilon} \int_0^1 dy \left[ -2\beta^2 y^2 + 2\beta^2 y + \frac{1-\beta^2}{2} \right]^{-1-\epsilon}. \end{aligned} \quad (40)$$

The integral over  $x$  in Eq. (40) contains both UV and IR singularities. We isolate the UV singularities and find that

$$\int_0^1 dx x^{-1+2\epsilon} (1-x)^{-1-2\epsilon} = \frac{1}{2\epsilon} + \text{IR}. \quad (41)$$

The integral over  $y$  is given in terms of hypergeometric functions  ${}_2F_1\left(-\epsilon, 1+\epsilon, 1-\epsilon, \frac{1+\beta}{2}\right)$  which can be expanded in powers of  $\epsilon$ . After some calculation, we find

$$\begin{aligned} \int \frac{d^n k}{v_i \cdot k v_j \cdot k (k^2)^{1+\epsilon/2}} &= \frac{2i\pi^2}{\beta\epsilon} \ln\left(\frac{1-\beta}{1+\beta}\right) + \frac{2i\pi^2}{\beta} \left[ \text{Li}_2\left(\frac{2}{1+\beta}\right) - \text{Li}_2\left(\frac{2}{1-\beta}\right) \right] \\ &+ \ln^2(1+\beta) - \ln^2(1-\beta) + \frac{1}{2}(6\ln 2 - \ln \pi - \gamma_E) \ln\left(\frac{1-\beta}{1+\beta}\right). \end{aligned} \quad (42)$$

Assembling everything together we find the result for the UV poles of  $I_{2l}^b$ ,

$$\begin{aligned} I_{2l}^{bUV} &= \pi^4 \frac{(1+\beta^2)}{\beta} \left\{ \frac{1}{\epsilon^2} \ln\left(\frac{1-\beta}{1+\beta}\right) + \frac{1}{\epsilon} \left[ \text{Li}_2\left(\frac{2}{1+\beta}\right) - \text{Li}_2\left(\frac{2}{1-\beta}\right) \right] \right. \\ &\left. + \ln^2(1+\beta) - \ln^2(1-\beta) + (1+3\ln 2 - \ln \pi - \gamma_E) \ln\left(\frac{1-\beta}{1+\beta}\right) \right\}. \end{aligned} \quad (43)$$

We continue with the evaluation of  $I_{2l}^c$ . Now

$$\begin{aligned} \int d^n l \frac{l^\mu l^\nu}{l^2(l-k)^2} &= i\pi^{2-\epsilon/2} \Gamma\left(\frac{\epsilon}{2}\right) \Gamma\left(1-\frac{\epsilon}{2}\right) \frac{\Gamma\left(3-\frac{\epsilon}{2}\right)}{\Gamma(4-\epsilon)} (k^2)^{-\epsilon/2} k^\mu k^\nu \\ &+ \frac{i\pi^{2-\epsilon/2}}{2} g^{\mu\nu} \Gamma\left(-1+\frac{\epsilon}{2}\right) \frac{(\Gamma(2-\frac{\epsilon}{2}))^2}{\Gamma(4-\epsilon)} (k^2)^{1-\epsilon/2} \end{aligned} \quad (44)$$

and after a few manipulations we find

$$I_{2l}^c = -i\pi^{2-\epsilon/2} \Gamma\left(-1+\frac{\epsilon}{2}\right) \frac{(\Gamma(2-\frac{\epsilon}{2}))^2}{\Gamma(4-\epsilon)} v_i \cdot v_j \int \frac{d^n k}{v_i \cdot k v_j \cdot k (k^2)^{1+\epsilon/2}}. \quad (45)$$

The integral over  $k$  was evaluated before for  $I_{10}^b$ , Eq. (40). We thus find that the UV poles of  $I_{10}^c$  are

$$I_{2l}^{cUV} = \pi^4 \frac{1+\beta^2}{3\beta} \left\{ -\frac{1}{\epsilon^2} \ln \left( \frac{1-\beta}{1+\beta} \right) + \frac{1}{\epsilon} \left[ -\text{Li}_2 \left( \frac{2}{1+\beta} \right) + \text{Li}_2 \left( \frac{2}{1-\beta} \right) - \ln^2(1+\beta) + \ln^2(1-\beta) + \left( -\frac{4}{3} - 3 \ln 2 + \ln \pi + \gamma_E \right) \ln \left( \frac{1-\beta}{1+\beta} \right) \right] \right\}. \quad (46)$$

Finally, we calculate  $I_{2l}^d$  and  $I_{2l}^e$ . We use Eq. (38) for the  $l$  integral and then find that the remaining integral over  $k$  vanishes, so  $I_{2l}^d = I_{2l}^e = 0$ .

Adding all the terms in Eq. (31), the final result for the UV poles of  $I_{2l}$  is

$$I_{2l}^{UV} = -n_f \frac{\alpha_s^2 (1+\beta^2)}{\pi^2 6\beta} \left\{ \frac{1}{\epsilon^2} \ln \left( \frac{1-\beta}{1+\beta} \right) + \frac{1}{\epsilon} \left[ \text{Li}_2 \left( \frac{2}{1+\beta} \right) - \text{Li}_2 \left( \frac{2}{1-\beta} \right) + \ln^2(1+\beta) - \ln^2(1-\beta) + \left( \frac{5}{6} + 5 \ln 2 + \ln \pi - \gamma_E \right) \ln \left( \frac{1-\beta}{1+\beta} \right) \right] \right\}. \quad (47)$$

More results for two-loop integrals with massive quarks will appear in [23].

## 5 Small- $x$ resummations

In the last forty years there has been a large effort trying to understand what are the correct effective degrees of freedom underlying the strong interaction at high energies. In scattering processes where the center-of-mass energy is much larger than any other scales the Balitsky-Fadin-Kuraev-Lipatov (BFKL) approach [10–14] emerges as the correct approach to describe the scattering. This framework relies upon  $t$ -channel “Reggeized” gluons interacting with each other via standard gluons in the  $s$ -channel and a gauge invariant three particle vertex. This simple structure is a consequence of using multi-Regge kinematics where gluon cascades are ordered in longitudinal components but with a random walk in transverse momenta. Although this simple iterative and linear structure must be modified at higher energies in order to introduce unitarization and non-linear corrections, there is a window at present and future colliders where the BFKL predictions hold.

In the leading logarithmic approximation (LLA) we resum terms of the form  $(\alpha_s \ln s)^n$ . Diagrams contributing to the running of the strong coupling do not appear and the coupling is a constant parameter. The factor needed to scale the energy in the logarithms is also free and the predictability of the LL approximation is limited. In the next-to-leading logarithmic approximation (NLLA) diagrams with an extra power in the coupling without introducing an extra logarithm in energy are considered. The coupling is allowed to run and the energy scale is determined.

In this contribution we discuss three aspects of the BFKL resummation program. In subsection 5.1 we review the relevant equations to describe final states at small values of Bjorken  $x$  in Deep Inelastic Scattering (DIS). We introduce the concept of color coherence and the CCFM equation. We show the differences and similarities between the BFKL

approach and the introduction of angular ordering in the case of jet rates. In subsection 5.2 we analyse in detail how to extend the region of applicability of the multi-Regge kinematics, the basic ingredient in the BFKL approach, to regions with collinear emissions. We will find an interesting structure in the higher-order corrections that can be resummed into a Bessel function of the first kind, which accounts for the double logarithms in transverse scales. In subsection 5.3 we briefly explain the  $SL(2, C)$  invariance associated to the BFKL Hamiltonian and how it shows up in the physics of multijet events, in particular in the production of Mueller-Navelet jets at a hadron collider.

## 5.1 QCD coherence and small- $x$ final states

In Quantum Electrodynamics coherence effects are responsible for the suppression of soft bremsstrahlung from electron-positron pairs. In QCD processes such as  $g \rightarrow q\bar{q}$  any soft gluon emitted with an angle from one of the fermionic lines larger than the angle of emission in the  $q\bar{q}$  pair will probe the total color charge of the pair. This charge is the same as the one from the parent gluon and the radiation takes place as if the soft gluon was emitted from it. This color coherence leads to the angular ordering of sequential gluon emissions.

In DIS, let us say that the  $(i-1)$ th emitted gluon from the proton has energy  $E_{i-1}$ . A gluon radiated from it with a fraction  $(1-z_i)$  of its energy and a transverse momentum  $q_i$  will have an opening angle

$$\theta_i \approx \frac{q_i}{(1-z_i)E_{i-1}}, \quad (48)$$

with

$$z_i = \frac{E_i}{E_{i-1}}. \quad (49)$$

Color coherence leads to angular ordering with increasing opening angles towards the hard scale (the photon). Therefore, we have  $\theta_{i+1} > \theta_i$ , or

$$\frac{q_{i+1}}{1-z_{i+1}} > \frac{z_i q_i}{1-z_i}, \quad (50)$$

which in the limit  $z_i, z_{i+1} \ll 1$  reduces to

$$q_{i+1} > z_i q_i. \quad (51)$$

In Ref. [58–61] the BFKL equation for the unintegrated structure function was obtained in a form suitable for the study of exclusive observables:

$$f_\omega(\mathbf{k}) = f_\omega^0(\mathbf{k}) + \bar{\alpha}_S \int \frac{d^2 \mathbf{q}}{\pi q^2} \int_0^1 \frac{dz}{z} z^\omega \Delta_R(z, k) \Theta(q - \mu) f_\omega(\mathbf{q} + \mathbf{k}), \quad (52)$$

where  $\mu$  is a collinear cutoff,  $\mathbf{q}$  is the transverse momentum of the emitted gluon, and the gluon Regge factor is

$$\Delta_R(z_i, k_i) = \exp \left[ -\bar{\alpha}_S \ln \frac{1}{z_i} \ln \frac{k_i^2}{\mu^2} \right], \quad (53)$$

with  $k_i \equiv |\mathbf{k}_i|$ , and  $\bar{\alpha}_S \equiv \alpha_S N_c / \pi$ . Under iteration, this expression generates real gluon emissions with all the virtual corrections summed to all orders. Since  $f_\omega$  is an inclusive structure function, it includes the sum over all final states and the  $\mu$ -dependence cancels between the real and virtual contributions.

The structure function is defined by integrating over all  $\mu^2 \leq q_i^2 \leq Q^2$ , *i.e.*

$$F_{0\omega}(Q, \mu) \equiv \Theta(Q - \mu) + \sum_{r=1}^{\infty} \int_{\mu^2}^{Q^2} \prod_{i=1}^r \frac{d^2 \mathbf{q}_i}{\pi q_i^2} dz_i \frac{\bar{\alpha}_S}{z_i} z_i^\omega \Delta_R(z_i, k_i), \quad (54)$$

with  $i$  real gluon emissions in each iteration of the kernel. The contributions from a fixed number  $r$  of emitted gluons is

$$F_{0\omega}(Q) = \int_0^1 dx x^\omega F_0(x, Q) = 1 + \sum_{r=1}^{\infty} F_{0\omega}^{(r)}(Q). \quad (55)$$

In Ref. [59] the perturbative expansion for the  $F_{0\omega}^{(r)}(Q, \mu)$

$$F_{0\omega}^{(r)}(Q, \mu) = \sum_{n=r}^{\infty} C_0^{(r)}(n; T) \frac{\bar{\alpha}_S^n}{\omega^n}, \quad (56)$$

was obtained with  $T \equiv \ln(Q/\mu)$ . Then we have

$$F_{0\omega}(Q) \equiv \sum_{i=0}^{\infty} F_{0\omega}^{(i)}(Q) = \left( \frac{Q^2}{\mu^2} \right)^{\bar{\gamma}}, \quad (57)$$

where  $\bar{\gamma}$  is the BFKL anomalous dimension. It was pointed out that coherence effects significantly modify the individual  $F_{0\omega}^{(r)}(Q)$  whilst preserving the sum  $F_{0\omega}(Q)$ , and care must be taken to account properly for coherence in the calculation of associated distributions.

Modifying the BFKL formalism to account for coherence [58–61],  $F_{0\omega}(Q, \mu)$  becomes

$$F_\omega(Q, \mu) = \Theta(Q - \mu) + \sum_{r=1}^{\infty} \int_0^{Q^2} \prod_{i=1}^r \frac{d^2 \mathbf{q}_i}{\pi q_i^2} dz_i \frac{\bar{\alpha}_S}{z_i} z_i^\omega \Delta(z_i, q_i, k_i) \Theta(q_i - z_{i-1} q_{i-1}), \quad (58)$$

where  $\Delta_R(z_i, k_i)$  is substituted by

$$\Delta(z_i, q_i, k_i) = \exp \left[ -\bar{\alpha}_S \ln \frac{1}{z_i} \ln \frac{k_i^2}{z_i q_i^2} \right]; \quad k_i > q_i, \quad (59)$$

and for the first emission we take  $q_0 z_0 = \mu$ . The expansion of  $F_\omega^{(r)}(Q)$  is now

$$F_\omega^{(r)}(Q) = \sum_{n=r}^{\infty} \sum_{m=1}^n C^{(r)}(n, m; T) \frac{\bar{\alpha}_S^n}{\omega^{2n-m}}. \quad (60)$$

A collinear cutoff is needed only on the emission of the first gluon because subsequent collinear emissions are regulated by the angular ordering constraint.

The rates for the emission of a fixed number of resolved gluons, with a transverse momentum larger than a resolution scale  $\mu_R$ , together with any number of unresolved ones, were calculated in Ref. [62] in the LLA, to third order in  $\bar{\alpha}_S$ .  $\mu_R$  is constrained by the collinear cutoff and the hard scale,  $\mu \ll \mu_R \ll Q$ . For the  $n$ -jet rate all the graphs with  $n$  resolved gluons and any number of unresolvable ones were considered. Expanding the Regge factors to  $\mathcal{O}(\bar{\alpha}_S^3)$  we find that the jet rates both in the multi-Regge (BFKL) approach and in the coherent (CCFM) approach are the same:

$$0 \text{ jet} = \frac{(2\bar{\alpha}_S)}{\omega} S + \frac{(2\bar{\alpha}_S)^2}{\omega^2} \left[ \frac{S^2}{2} \right] + \frac{(2\bar{\alpha}_S)^3}{\omega^3} \left[ \frac{S^3}{6} \right], \quad (61)$$

$$1 \text{ jet} = \frac{(2\bar{\alpha}_S)}{\omega} T + \frac{(2\bar{\alpha}_S)^2}{\omega^2} \left[ TS - \frac{1}{2} T^2 \right] + \frac{(2\bar{\alpha}_S)^3}{\omega^3} \left[ \frac{1}{3} T^3 - \frac{1}{2} T^2 S + \frac{1}{2} T S^2 \right], \quad (62)$$

$$2 \text{ jet} = \frac{(2\bar{\alpha}_S)^2}{\omega^2} [T^2] + \frac{(2\bar{\alpha}_S)^3}{\omega^3} \left[ T^2 S - \frac{7}{6} T^3 \right], \quad (63)$$

$$3 \text{ jet} = \frac{(2\bar{\alpha}_S)^3}{\omega^3} [T^3], \quad (64)$$

with  $T = \ln(Q/\mu_R)$  and  $S = \ln(\mu_R/\mu)$ . When coherence is introduced the singularities at  $\omega \sim 0$  are stronger than in the BFKL approach but the extra logarithms cancel in the sum of all the graphs needed for the jet rates. The net effect is that the final results are the same as those obtained without coherence [62]. This is true to all orders in the coupling [63] since a generating function for the jet multiplicity distribution was obtained in [64]. Within the multi-Regge kinematics the  $r$ -jet rate reads

$$R_\omega^{(n \text{ jet})}(Q, \mu_R) = \frac{F_\omega^{(n \text{ jet})}(Q, \mu_R, \mu)}{F_\omega(Q, \mu)} = \frac{1}{n!} \frac{\partial^n}{\partial u^n} R_\omega(u, T) \Big|_{u=0}, \quad (65)$$

where the jet-rate generating function  $R_\omega$  is given by

$$R_\omega(u, T) = \exp \left( -\frac{2\bar{\alpha}_s}{\omega} T \right) \left[ 1 + (1-u) \frac{2\bar{\alpha}_s}{\omega} T \right]^{\frac{u}{1-u}}. \quad (66)$$

The same generating function is obtained when coherence is considered. The mean number of jets and the mean square fluctuation in this number are

$$\langle n \rangle = \frac{\partial}{\partial u} R_\omega(u, T) \Big|_{u=1} = \frac{2\bar{\alpha}_s}{\omega} T + \frac{1}{2} \left( \frac{2\bar{\alpha}_s}{\omega} T \right)^2, \quad (67)$$

$$\langle n^2 \rangle - \langle n \rangle^2 = \frac{2\bar{\alpha}_s}{\omega} T + \frac{3}{2} \left( \frac{2\bar{\alpha}_s}{\omega} T \right)^2 + \frac{2}{3} \left( \frac{2\bar{\alpha}_s}{\omega} T \right)^3. \quad (68)$$

In general, the  $p$ th central moment of the jet multiplicity distribution is a polynomial in  $\bar{\alpha}_s T/\omega$  of degree  $2p - 1$ , indicating that the distribution becomes relatively narrow in the limit of very small  $x$  and large  $Q/\mu_R$  [64].

In Ref. [65, 66] the subject was developed even further and all subleading logarithms of  $Q^2/\mu_R^2$  were included to calculate the jet multiplicity in Higgs production at the LHC. In Ref. [65] they extended the results from a  $[\bar{\alpha}_s \ln(1/x) \ln(Q^2/\mu_R^2)]^n$  resummation to a  $[\bar{\alpha}_s \ln(1/x)]^n [\ln(Q^2/\mu_R^2)]^m$  one with  $0 < m \leq n$ , proving that the quadratic and cubic forms of the mean and the variance remain valid. It has also been shown that for any sufficiently inclusive observables the CCFM formalism leads to the same results as the BFKL equation [67]. The key idea to understand this result comes if we try to obtain the results of Ref. [59] from those in the previous section in the limit  $\mu_R \rightarrow 0$ . To get the right solution we should consider subleading terms  $\bar{\alpha}_s \ln^2(Q/\mu_R)$  which must be resummed when taking the limit  $\mu_R \rightarrow 0$  to obtain a continuous transition from the case where BFKL and CCFM results are equivalent, to that of them being different. If we also consider the effects of introducing the  $z \rightarrow 1$  divergent part of the splitting function in the CCFM approach we will see that this leads to all BFKL and CCFM final-state properties being identical in the  $[\bar{\alpha}_s \ln(1/x) \ln(Q^2/\mu_R^2)]^n$  approximation [67]. Recent reviews devoted to the implementation of CCFM in Monte Carlo event generators can be found in, *e.g.*, [68–71]. An approach which has the potential to apply BFKL in the NLLA to DIS phenomenology is that in Ref. [72–75]. In the NLLA approximation it is important to carefully take into account  $k_t$  factorization [76].

## 5.2 Improving the collinear region of multi-Regge kinematics

In this section we revisit the approach of Ref. [77] where the multi-Regge kinematics was extended to include collinear contributions present to all orders in the BFKL formalism. In Ref. [78] the structure in transverse momentum space of the double logarithms resummed was explicitly extracted. A new renormalization group (RG)-improved kernel was obtained which does not mix transverse with longitudinal momentum components.

In the  $\overline{\text{MS}}$  renormalisation scheme, the BFKL kernel in the NLLA acting on a smooth function [15, 16] is

$$\begin{aligned} \int d^2 \vec{q}_2 \mathcal{K}(\vec{q}_1, \vec{q}_2) f(q_2^2) = \\ \int \frac{d^2 \vec{q}_2}{|q_1^2 - q_2^2|} \left\{ \left[ \bar{\alpha}_s + \bar{\alpha}_s^2 \left( \mathcal{S} - \frac{\beta_0}{4N_c} \ln \left( \frac{|q_1^2 - q_2^2|^2}{\max(q_1^2, q_2^2) \mu^2} \right) \right) \right] \right. \\ \left. \times \left( f(q_2^2) - 2 \frac{\min(q_1^2, q_2^2)}{(q_1^2 + q_2^2)} f(q_1^2) \right) - \frac{\bar{\alpha}_s^2}{4} \left( \mathcal{T}(q_1^2, q_2^2) + \ln^2 \left( \frac{q_1^2}{q_2^2} \right) \right) f(q_2^2) \right\}, \quad (69) \end{aligned}$$

where  $\beta_0 = (11N_c - 2n_f)/3$ ,  $\mathcal{S} = (4 - \pi^2 + 5\beta_0/N_c)/12$ , and  $\mathcal{T}(q_1^2, q_2^2)$  can be found in Ref. [15]. The collinear structure can be obtained acting on the eigenfunctions in the LLA, *i.e.*

$$\int d^2 \vec{q}_2 \mathcal{K}(\vec{q}_1, \vec{q}_2) \left( \frac{\bar{\alpha}_s(q_2^2)}{\bar{\alpha}_s(q_1^2)} \right)^{-\frac{1}{2}} \left( \frac{q_2^2}{q_1^2} \right)^{\gamma-1} = \bar{\alpha}_s(q_1^2) \chi_0(\gamma) + \bar{\alpha}_s^2 \chi_1(\gamma). \quad (70)$$

Here we have

$$\chi_0(\gamma) = 2\psi(1) - \psi(\gamma) - \psi(1-\gamma), \quad (71)$$

$$\begin{aligned} \chi_1(\gamma) = & \mathcal{S}\chi_0(\gamma) + \frac{1}{4}(\psi''(\gamma) + \psi''(1-\gamma)) - \frac{1}{4}(\phi(\gamma) + \phi(1-\gamma)) \\ & - \frac{\pi^2 \cos(\pi\gamma)}{4\sin^2(\pi\gamma)(1-2\gamma)} \left( 3 + \left( 1 + \frac{n_f}{N_c^3} \right) \frac{(2+3\gamma(1-\gamma))}{(3-2\gamma)(1+2\gamma)} \right) + \frac{3}{2}\zeta_3 - \frac{\beta_0}{8N_c}\chi_0^2(\gamma), \end{aligned} \quad (72)$$

with  $\psi(\gamma) = \Gamma'(\gamma)/\Gamma(\gamma)$  and

$$\begin{aligned} \phi(\gamma) + \phi(1-\gamma) = & \sum_{m=0}^{\infty} \left( \frac{1}{\gamma+m} + \frac{1}{1-\gamma+m} \right) \left( \psi' \left( \frac{2+m}{2} \right) - \psi' \left( \frac{1+m}{2} \right) \right). \end{aligned} \quad (73)$$

The pole structure around  $\gamma = 0, 1$  is

$$\chi_0(\gamma) \simeq \frac{1}{\gamma} + \{\gamma \rightarrow 1-\gamma\}, \quad (74)$$

$$\chi_1(\gamma) \simeq \frac{a}{\gamma} + \frac{b}{\gamma^2} - \frac{1}{2\gamma^3} + \{\gamma \rightarrow 1-\gamma\} \quad (75)$$

with

$$a = \frac{5}{12} \frac{\beta_0}{N_c} - \frac{13}{36} \frac{n_f}{N_c^3} - \frac{55}{36}, \quad b = -\frac{1}{8} \frac{\beta_0}{N_c} - \frac{n_f}{6N_c^3} - \frac{11}{12}. \quad (76)$$

The cubic poles stem from  $\psi''$  and compensate for the equivalent terms appearing when the Regge-like energy scale  $s_0 = q_1 q_2$  is shifted to the DIS choice  $s_0 = q_{1,2}^2$ . Higher order terms beyond the NLLA, not compatible with RG evolution, are also generated by this change of scale. The NLLA truncation of the perturbative expansion is then the reason why the gluon Green's function develops oscillations, where the Green's function can have negative values, in the  $q_1^2/q_2^2$  ratio.

It is possible to remove the most dominant poles in  $\gamma$ -space incompatible with RG evolution by simply shifting the  $\omega$ -pole present in the BFKL scale invariant eigenfunction. Here we focus on the scheme proposed in Ref. [77]:

$$\begin{aligned} \omega = & \bar{\alpha}_s \left( 1 + \left( a + \frac{\pi^2}{6} \right) \bar{\alpha}_s \right) \left( 2\psi(1) - \psi \left( \gamma + \frac{\omega}{2} - b \bar{\alpha}_s \right) - \psi \left( 1 - \gamma + \frac{\omega}{2} - b \bar{\alpha}_s \right) \right) \\ & + \bar{\alpha}_s^2 \left( \chi_1(\gamma) + \left( \frac{1}{2}\chi_0(\gamma) - b \right) (\psi'(\gamma) + \psi'(1-\gamma)) - \left( a + \frac{\pi^2}{6} \right) \chi_0(\gamma) \right). \end{aligned} \quad (77)$$

We can approximately solve this equation considering the  $\omega$ -shift in the form

$$\omega = \bar{\alpha}_s (1 + A \bar{\alpha}_s) \left( 2\psi(1) - \psi \left( \gamma + \frac{\omega}{2} + B \bar{\alpha}_s \right) - \psi \left( 1 - \gamma + \frac{\omega}{2} + B \bar{\alpha}_s \right) \right), \quad (78)$$



which can be written as

$$\omega = \bar{\alpha}_s (1 + A\bar{\alpha}_s) \sum_{m=0}^{\infty} \left( \frac{1}{\gamma + m + \frac{\omega}{2} + B\bar{\alpha}_s} + \frac{1}{1 - \gamma + m + \frac{\omega}{2} + B\bar{\alpha}_s} - \frac{2}{m+1} \right). \quad (79)$$

The solution to this shift can be obtained by adding all the approximated solutions at the different poles plus a term related to the virtual contributions, *i.e.*

$$\begin{aligned} \omega = & \sum_{m=0}^{\infty} \left\{ -(1 + 2m + 2B\bar{\alpha}_s) + |\gamma + m + B\bar{\alpha}_s| \left( 1 + \frac{2\bar{\alpha}_s(1 + A\bar{\alpha}_s)}{(\gamma + m + B\bar{\alpha}_s)^2} \right)^{\frac{1}{2}} \right. \\ & \left. + |1 - \gamma + m + B\bar{\alpha}_s| \left( 1 + \frac{2\bar{\alpha}_s(1 + A\bar{\alpha}_s)}{(1 - \gamma + m + B\bar{\alpha}_s)^2} \right)^{\frac{1}{2}} - \frac{2\bar{\alpha}_s(1 + A\bar{\alpha}_s)}{m+1} \right\}. \quad (80) \end{aligned}$$

At the  $\gamma = 0, 1$  poles this expansion generates the NLLA terms:

$$\omega \simeq \frac{\bar{\alpha}_s}{\gamma} + \bar{\alpha}_s^2 \left( \frac{A}{\gamma} - \frac{B}{\gamma^2} - \frac{1}{2\gamma^3} \right) + \{\gamma \rightarrow 1 - \gamma\}. \quad (81)$$

To match the original kernel at NLLA we set  $A = a$  and  $B = -b$  from Eq. (76).

We now include the full NLLA scale invariant kernel without double counting terms:

$$\begin{aligned} \omega = & \bar{\alpha}_s \chi_0(\gamma) + \bar{\alpha}_s^2 \chi_1(\gamma) \\ & + \left\{ \sum_{m=0}^{\infty} \left[ \left( \sum_{n=0}^{\infty} \frac{(-1)^n (2n)!}{2^n n! (n+1)!} \frac{(\bar{\alpha}_s + a\bar{\alpha}_s^2)^{n+1}}{(\gamma + m - b\bar{\alpha}_s)^{2n+1}} \right) \right. \right. \\ & \left. \left. - \frac{\bar{\alpha}_s}{\gamma + m} - \bar{\alpha}_s^2 \left( \frac{a}{\gamma + m} + \frac{b}{(\gamma + m)^2} - \frac{1}{2(\gamma + m)^3} \right) \right] + \{\gamma \rightarrow 1 - \gamma\} \right\}. \quad (82) \end{aligned}$$

This result reproduces the  $\omega$ -shift very closely, see Fig. 9. The imaginary part of  $\gamma$  at the maximum of the NLLA scale invariant eigenvalue (middle plot of Fig. 9) is not zero and results in oscillations in the  $q_1^2/q_2^2$  variable. These are eliminated when the RG-improved kernel is used, as it also happens for the “all-poles” kernel.

It is very important to note that in Eq. (82) the  $\omega$ -space is decoupled from the  $\gamma$ -representation. In Ref. [78] an expression for the collinearly improved BFKL kernel which does not mix longitudinal with transverse degrees of freedom was found. The only modification needed in the full NLLA kernel to introduce the “all-poles” resummation is to remove the term

$$- \frac{\bar{\alpha}_s^2}{4} \frac{1}{(\vec{q} - \vec{k})^2} \ln^2 \left( \frac{q^2}{k^2} \right) \quad (83)$$

in the real emission kernel,  $\mathcal{K}_r(\vec{q}, \vec{k})$ , and replace it with

$$\frac{1}{(\vec{q} - \vec{k})^2} \left\{ \left( \frac{q^2}{k^2} \right)^{-b\bar{\alpha}_s \frac{|k-q|}{k-q}} \sqrt{\frac{2(\bar{\alpha}_s + a\bar{\alpha}_s^2)}{\ln^2 \left( \frac{q^2}{k^2} \right)}} J_1 \left( \sqrt{2(\bar{\alpha}_s + a\bar{\alpha}_s^2) \ln^2 \left( \frac{q^2}{k^2} \right)} \right) \right\}$$

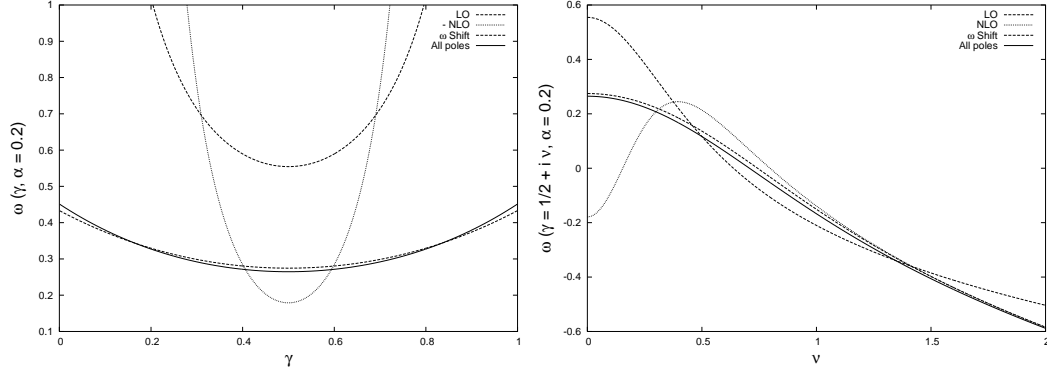


Figure 9:  $\gamma$ -representation of the LLA and NLLA kernels. The RG-improved kernel by a  $\omega$ -shift is included together with the new “all-poles” approximation.

$$-\bar{\alpha}_s - a \bar{\alpha}_s^2 + b \bar{\alpha}_s^2 \frac{|k-q|}{k-q} \ln \left( \frac{q^2}{k^2} \right) \Bigg\}, \quad (84)$$

with  $J_1$  the Bessel function of the first kind. When the difference between the  $q^2$  and  $k^2$  scales is not very large then

$$J_1 \left( \sqrt{2\bar{\alpha}_s \ln^2 \left( \frac{q^2}{k^2} \right)} \right) \simeq \sqrt{\frac{\bar{\alpha}_s}{2} \ln^2 \left( \frac{q^2}{k^2} \right)}, \quad (85)$$

and its influence is minimal, not affecting the “Regge-like” region. When the ratio of transverse momenta becomes larger then

$$J_1 \left( \sqrt{2\bar{\alpha}_s \ln^2 \left( \frac{q^2}{k^2} \right)} \right) \simeq \left( \frac{2}{\pi^2 \bar{\alpha}_s \ln^2 \left( \frac{q^2}{k^2} \right)} \right)^{\frac{1}{4}} \cos \left( \sqrt{2\bar{\alpha}_s \ln^2 \left( \frac{q^2}{k^2} \right)} - \frac{3\pi}{4} \right) \quad (86)$$

compensating for the unphysical oscillations. This resummation of all-poles has been applied to extend the region of applicability of BFKL calculations in the NLLA in the case of electroproduction of light vector mesons in Ref. [79].

### 5.3 Conformal signatures at the Large Hadron Collider: azimuthal angle

We now proceed to review the work of Ref. [80] where azimuthal angle decorrelations in inclusive dijet cross sections were studied analytically to include the NLLA to the BFKL kernel, while keeping the jet vertices at leading order. It was shown how the angular decorrelation for jets with a wide relative separation in rapidity largely decreases when higher order effects are considered.

Observables where BFKL effects should be dominant require a large enough center-of-mass energy, and two large and similar transverse scales. An example is the inclusive

hadroproduction of two jets with large and similar transverse momenta and a large relative separation in rapidity,  $Y$ , the so-called Mueller-Navelet jets, first proposed in Ref. [81]. A rise with  $Y$  in the partonic cross section was predicted in agreement with the LLA hard Pomeron intercept. At the hadronic level, Mueller-Navelet jets are produced in a region where the parton distribution falls very quickly, reducing this rise. Small  $x$  resummation effects are very relevant if we investigate the azimuthal angle decorrelation of the pair of jets. BFKL enhances soft real emission as  $Y$  increases, reducing the angular correlation. This was first investigated in the LLA in Ref. [82–84]. The rate of decorrelation in the LLA lies quite below the experimental data [85–88] at the Tevatron. This motivates the NLLA discussion of this subsection.

We are interested in the cross section  $\text{parton} + \text{parton} \rightarrow \text{jet} + \text{jet} + \text{soft emission}$ , with the two jets having transverse momenta  $\vec{q}_1$  and  $\vec{q}_2$  and with a relative rapidity separation  $Y$ . The differential partonic cross section is

$$\frac{d\hat{\sigma}}{d^2\vec{q}_1 d^2\vec{q}_2} = \frac{\pi^2 \bar{\alpha}_s^2}{2} \frac{f(\vec{q}_1, \vec{q}_2, Y)}{q_1^2 q_2^2}. \quad (87)$$

It is useful to introduce a Mellin transform:

$$f(\vec{q}_1, \vec{q}_2, Y) = \int \frac{d\omega}{2\pi i} e^{\omega Y} f_\omega(\vec{q}_1, \vec{q}_2). \quad (88)$$

The solution to the BFKL equation in the LLA is

$$f_\omega(\vec{q}_1, \vec{q}_2) = \frac{1}{2\pi^2} \sum_{n=-\infty}^{\infty} \int_{-\infty}^{\infty} d\nu \left(q_1^2\right)^{-i\nu-\frac{1}{2}} \left(q_2^2\right)^{i\nu-\frac{1}{2}} \frac{e^{in(\theta_1-\theta_2)}}{\omega - \bar{\alpha}_s \chi_0(|n|, \nu)} \quad (89)$$

with

$$\chi_0(n, \nu) = 2\psi(1) - \psi\left(\frac{1}{2} + i\nu + \frac{n}{2}\right) - \psi\left(\frac{1}{2} - i\nu + \frac{n}{2}\right). \quad (90)$$

The nonforward BFKL equation corresponds to a Schrödinger-like equation with a holomorphically separable Hamiltonian where  $-iY$  is the time variable. Both the holomorphic and antiholomorphic sectors are invariant under spin zero Möbius transformations with eigenfunctions carrying a conformal weight of the form  $\gamma = \frac{1}{2} + i\nu + \frac{n}{2}$ . In the principal series of the unitary representation,  $\nu$  is real and  $|n|$  the integer conformal spin [89]. In this way extracting information about  $n$  is equivalent to proving the conformal structure of high energy QCD.

We now integrate over the phase space of the two emitted gluons together with some general jet vertices, *i.e.*

$$\hat{\sigma}(\alpha_s, Y, p_{1,2}^2) = \int d^2\vec{q}_1 \int d^2\vec{q}_2 \Phi_{\text{jet}_1}(\vec{q}_1, p_1^2) \Phi_{\text{jet}_2}(\vec{q}_2, p_2^2) \frac{d\hat{\sigma}}{d^2\vec{q}_1 d^2\vec{q}_2}. \quad (91)$$

In the jet vertices only leading-order terms are kept:

$$\Phi_{\text{jet}_i}^{(0)}(\vec{q}, p_i^2) = \theta(q^2 - p_i^2), \quad (92)$$

where  $p_i^2$  corresponds to a resolution scale for the transverse momentum of the gluon jet. To extend this analysis it is needed to use the NLO jet vertices in Ref. [90, 91] where the definition of a jet is much more complex than Eq. (92). We then have

$$\hat{\sigma}(\alpha_s, Y, p_{1,2}^2) = \frac{\pi^2 \bar{\alpha}_s^2}{2} \int d^2 \vec{q}_1 \int d^2 \vec{q}_2 \frac{\Phi_{\text{jet}_1}^{(0)}(\vec{q}_1, p_1^2)}{q_1^2} \frac{\Phi_{\text{jet}_2}^{(0)}(\vec{q}_2, p_2^2)}{q_2^2} f(\vec{q}_1, \vec{q}_2, Y). \quad (93)$$

In a transverse momenta operator representation:

$$\langle \vec{q} | \nu, n \rangle = \frac{1}{\pi \sqrt{2}} (q^2)^{i\nu - \frac{1}{2}} e^{in\theta}, \quad (94)$$

the action of the NLO kernel, calculated in Ref. [92], is

$$\begin{aligned} \hat{K} | \nu, n \rangle &= \left\{ \bar{\alpha}_s \chi_0(|n|, \nu) + \bar{\alpha}_s^2 \chi_1(|n|, \nu) \right. \\ &\quad \left. + \bar{\alpha}_s^2 \frac{\beta_0}{8N_c} \left[ 2 \chi_0(|n|, \nu) \left( i \frac{\partial}{\partial \nu} + \log \mu^2 \right) + \left( i \frac{\partial}{\partial \nu} \chi_0(|n|, \nu) \right) \right] \right\} | \nu, n \rangle, \end{aligned} \quad (95)$$

where  $\chi_1$ , for a general conformal spin, reads

$$\begin{aligned} \chi_1(n, \gamma) &= \mathcal{S} \chi_0(n, \gamma) + \frac{3}{2} \zeta(3) - \frac{\beta_0}{8N_c} \chi_0^2(n, \gamma) \\ &\quad + \frac{1}{4} \left[ \psi'' \left( \gamma + \frac{n}{2} \right) + \psi'' \left( 1 - \gamma + \frac{n}{2} \right) - 2 \phi(n, \gamma) - 2 \phi(n, 1 - \gamma) \right] \\ &\quad - \frac{\pi^2 \cos(\pi \gamma)}{4 \sin^2(\pi \gamma) (1 - 2\gamma)} \left\{ \left[ 3 + \left( 1 + \frac{n_f}{N_c^3} \right) \frac{2 + 3\gamma(1 - \gamma)}{(3 - 2\gamma)(1 + 2\gamma)} \right] \delta_{n0} \right. \\ &\quad \left. - \left( 1 + \frac{n_f}{N_c^3} \right) \frac{\gamma(1 - \gamma)}{2(3 - 2\gamma)(1 + 2\gamma)} \delta_{n2} \right\}. \end{aligned} \quad (96)$$

The function  $\phi$  can be found in Ref. [92].

The jet vertices on the basis in Eq. (94) are:

$$\int d^2 \vec{q} \frac{\Phi_{\text{jet}_1}^{(0)}(\vec{q}, p_1^2)}{q^2} \langle \vec{q} | \nu, n \rangle = \frac{1}{\sqrt{2}} \frac{1}{\left( \frac{1}{2} - i\nu \right)} (p_1^2)^{i\nu - \frac{1}{2}} \delta_{n,0} \equiv c_1(\nu) \delta_{n,0}, \quad (97)$$

with the  $c_2(\nu)$  projection of  $\Phi_{\text{jet}_2}^{(0)}$  on  $\langle n, \nu | \vec{q} \rangle$  being the complex conjugate of (97) with  $p_1^2$  being replaced by  $p_2^2$ . The cross section can then be rewritten as

$$\begin{aligned} \hat{\sigma}(\alpha_s, Y, p_{1,2}^2) &= \frac{\pi^2 \bar{\alpha}_s^2}{2} \sum_{n=-\infty}^{\infty} \int_{-\infty}^{\infty} d\nu e^{\bar{\alpha}_s \chi_0(|n|, \nu) Y} c_1(\nu) c_2(\nu) \delta_{n,0} \\ &\quad \times \left\{ 1 + \bar{\alpha}_s^2 Y \left[ \chi_1(|n|, \nu) + \frac{\beta_0}{4N_c} \left( \log(\mu^2) + \frac{i}{2} \frac{\partial}{\partial \nu} \log \left( \frac{c_1(\nu)}{c_2(\nu)} \right) + \frac{i}{2} \frac{\partial}{\partial \nu} \right) \chi_0(|n|, \nu) \right] \right\}. \end{aligned} \quad (98)$$

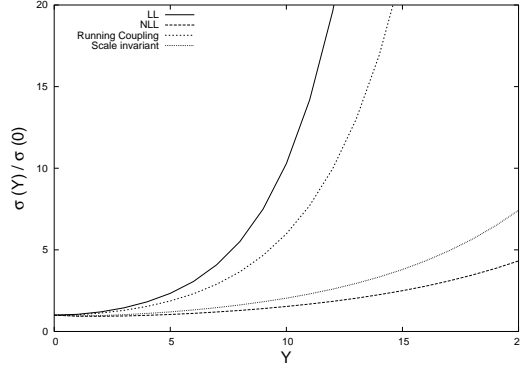


Figure 10: Evolution of the partonic cross section with the rapidity separation of the dijets.

For the LO jet vertices the logarithmic derivative in Eq. (98) is

$$-i \frac{\partial}{\partial \nu} \log \left( \frac{c_1(\nu)}{c_2(\nu)} \right) = \log(p_1^2 p_2^2) + \frac{1}{\frac{1}{4} + \nu^2}. \quad (99)$$

If  $\phi = \theta_1 - \theta_2 - \pi$ , in the case of two equal resolution momenta,  $p_1^2 = p_2^2 \equiv p^2$ , the angular differential cross section can be expressed as

$$\frac{d\hat{\sigma}(\alpha_s, Y, p^2)}{d\phi} = \frac{\pi^3 \bar{\alpha}_s^2}{2p^2} \frac{1}{2\pi} \sum_{n=-\infty}^{\infty} e^{in\phi} \mathcal{C}_n(Y), \quad (100)$$

with

$$\mathcal{C}_n(Y) = \int_{-\infty}^{\infty} \frac{d\nu}{2\pi} \frac{e^{\bar{\alpha}_s(p^2)Y \left( \chi_0(|n|, \nu) + \bar{\alpha}_s(p^2) \left( \chi_1(|n|, \nu) - \frac{\beta_0}{8N_c} \frac{\chi_0(|n|, \nu)}{\left(\frac{1}{4} + \nu^2\right)} \right) \right)}}{\left(\frac{1}{4} + \nu^2\right)}. \quad (101)$$

The coefficient governing the energy dependence of the cross section corresponds to  $n = 0$ :

$$\hat{\sigma}(\alpha_s, Y, p^2) = \frac{\pi^3 \bar{\alpha}_s^2}{2p^2} \mathcal{C}_0(Y). \quad (102)$$

We have chosen the resolution scale  $p = 30 \text{ GeV}$ ,  $n_f = 4$  and  $\Lambda_{\text{QCD}} = 0.1416 \text{ GeV}$ . The  $n = 0$  coefficient is directly related to the normalized cross section

$$\frac{\hat{\sigma}(Y)}{\hat{\sigma}(0)} = \frac{\mathcal{C}_0(Y)}{\mathcal{C}_0(0)}. \quad (103)$$

The rise with  $Y$  of this observable is shown in Fig. 10. Clearly the NLL intercept is very much reduced with respect to the LL case. The remaining coefficients with  $n \geq 1$  all decrease with  $Y$ . Because of this, the angular correlations also diminish as the rapidity

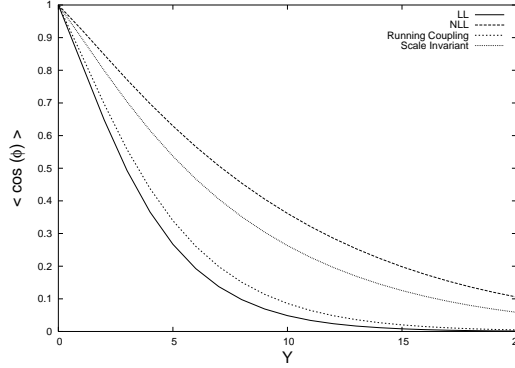


Figure 11: Dijet azimuthal angle decorrelation as a function of their separation in rapidity.

interval between the jets gets larger. This point can be studied in detail using the mean values

$$\langle \cos(m\phi) \rangle = \frac{\mathcal{C}_m(Y)}{\mathcal{C}_0(Y)}. \quad (104)$$

$\langle \cos(\phi) \rangle$  is calculated in Fig. 11. The NLL effects decrease the azimuthal angle decorrelation. This is the case for the running of the coupling and also for the scale invariant terms. This is encouraging from the phenomenological point of view given that the data at the Tevatron typically have lower decorrelation than predicted by LLA BFKL or LLA with running coupling. The difference in the decorrelation between LLA and NLLA is driven by the  $n = 0$  conformal spin since the ratio

$$\frac{\langle \cos(\phi) \rangle^{\text{NLLA}}}{\langle \cos(\phi) \rangle^{\text{LLA}}} = \frac{\mathcal{C}_1^{\text{NLLA}}(Y) \mathcal{C}_0^{\text{LLA}}(Y)}{\mathcal{C}_0^{\text{NLLA}}(Y) \mathcal{C}_1^{\text{LLA}}(Y)}, \quad (105)$$

remains in the region

$$1.2 > \frac{\mathcal{C}_1^{\text{NLLA}}(Y)}{\mathcal{C}_1^{\text{LLA}}(Y)} > 1. \quad (106)$$

This is a consequence of the good convergence, in terms of asymptotic intercepts of the NLLA BFKL calculation, for conformal spins larger than zero. For completeness the  $m = 2, 3$  cases for  $\langle \cos(m\phi) \rangle$  are shown in Fig. 12. These distributions test the structure of the higher conformal spins. The methods of this subsection have been applied to phenomenology of dijets at the Tevatron and the LHC in [93, 94], and to the production of forward jets in DIS at HERA in [95].

## 6 Conclusion

The precision of perturbative QCD calculations will play a major role in the confidence of new physics discoveries, both at this generation of experiments, Tevatron and LHC, and

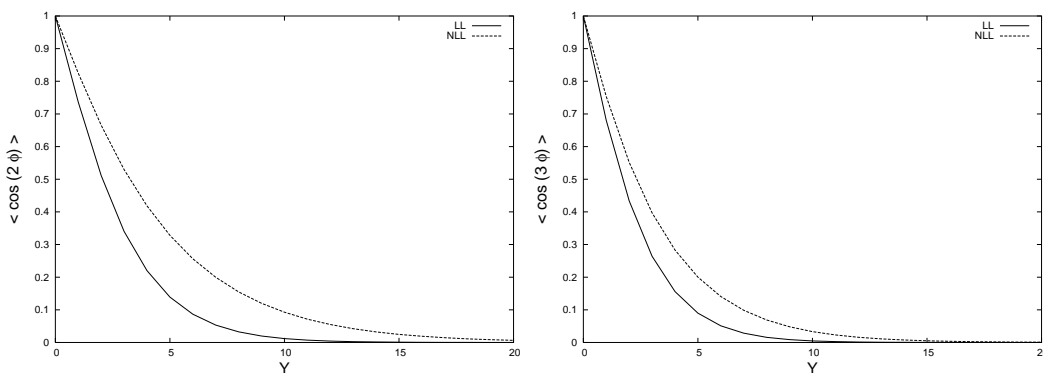


Figure 12: Dijet azimuthal angle decorrelation as a function of their separation in rapidity.

in future experiments. The most available avenue of improving the precision of QCD is through resummation of large contributions. We have presented results for the resummation of large- $x$  contributions and separately small- $x$  contributions. In both cases, the large contributions arise from incomplete cancellations of virtual and real terms, and can be computed in the eikonal approximation.

We have shown that the inclusion of soft-gluon corrections to top quark production cross sections is essential to stabilize the unphysical scale variations in the order-by-order calculations. This is necessary for any sort of precision calculation of the top mass and production channels. Additionally, we have shown the importance of resummation on  $W$  production at large transverse momentum, and on Higgs production. Discovery of the Higgs boson is the last remaining test of the Standard Model and precision measurements of its properties is essential to proceed forward with beyond the Standard Model theories.

We have also presented a framework to include collinear effects into the BFKL formalism. This stabilizes the oscillatory behavior that arises when one moves away from the strict kinematic regime of validity. It was shown how this inclusion improves the prediction of Mueller-Navalet jets, jets with a large rapidity separation but similar transverse scales. This is a process which will be observed at the LHC where the BFKL formalism should flourish; an important test of the complex behavior of QCD. A comparison between the predictions stemming from a pure BFKL analysis and one including QCD coherence in multijet final states in DIS has been also discussed in detail.

## Acknowledgements

The work of N.K. was supported by the National Science Foundation under Grant No. PHY 0555372.

## References

- [1] J.C. Collins, D.E. Soper, and G. Sterman, in *Perturbative Quantum Chromodynamics*, ed. A.H. Mueller (World Scientific, Singapore, 1989), p. 1.
- [2] G. Sterman, *Nucl. Phys. B* **281**, 310 (1987).
- [3] S. Catani and L. Trentadue, *Nucl. Phys. B* **327**, 323 (1989).
- [4] N. Kidonakis and G. Sterman, *Phys. Lett. B* **387**, 867 (1996); *Nucl. Phys. B* **505**, 321 (1997) [hep-ph/9705234].
- [5] H. Contopanagos, E. Laenen, and G. Sterman, *Nucl. Phys. B* **484**, 303 (1997) [hep-ph/9604313].
- [6] N. Kidonakis, G. Oderda, and G. Sterman, *Nucl. Phys. B* **525**, 299 (1998) [hep-ph/9801268].
- [7] N. Kidonakis, G. Oderda, and G. Sterman, *Nucl. Phys. B* **531**, 365 (1998) [hep-ph/9803241].
- [8] N. Kidonakis, *Int. J. Mod. Phys. A* **15**, 1245 (2000) [hep-ph/9902484].
- [9] E. Laenen, G. Oderda, and G. Sterman, *Phys. Lett. B* **438**, 173 (1998) [hep-ph/9806467].
- [10] L.N. Lipatov, *Sov. J. Nucl. Phys.* **23**, 338 (1976).
- [11] V.S. Fadin, E.A. Kuraev, and L.N. Lipatov, *Phys. Lett. B* **60**, 50 (1975).
- [12] E.A. Kuraev, L.N. Lipatov, and V.S. Fadin, *Sov. Phys. JETP* **44**, 443 (1976).
- [13] E.A. Kuraev, L.N. Lipatov, V.S. Fadin, *Sov. Phys. JETP* **45**, 199 (1977).
- [14] I.I. Balitsky and L.N. Lipatov, *Sov. J. Nucl. Phys.* **28**, 822 (1978).
- [15] V.S. Fadin and L.N. Lipatov, *Phys. Lett. B* **429**, 127 (1998) [hep-ph/9802290].
- [16] M. Ciafaloni and G. Camici, *Phys. Lett. B* **430**, 349 (1998) [hep-ph/9803389].
- [17] G.P. Korchemsky and A.V. Radyushkin, *Phys. Lett. B* **171**, 459 (1986); *Nucl. Phys. B* **283**, 342 (1987).
- [18] J. Botts and G. Sterman, *Nucl. Phys. B* **325**, 62 (1989).
- [19] G.P. Korchemsky, *Phys. Lett. B* **325**, 459 (1994) [hep-ph/9311294].
- [20] I.A. Korchemskaya and G.P. Korchemsky, *Nucl. Phys. B* **437**, 127 (1995) [hep-ph/9409446].



- 
- [21] S.M. Aybat, L.J. Dixon, and G. Sterman, *Phys. Rev. Lett.* **97**, 072001 (2006) [hep-ph/0606254]; *Phys. Rev. D* **74**, 074004 (2006) [hep-ph/0607309].
- [22] N. Kidonakis, hep-ph/0208056; in *Deep Inelastic Scattering, DIS 2003* (PNPI, Gatchina, 2003), p. 541 [hep-ph/0307145].
- [23] N. Kidonakis and P. Stephens, in preparation; in *Deep Inelastic Scattering and Related Subjects, DIS 2008* (Atlantis Press/SciWIPub, 2008), arXiv:0805.1193 [hep-ph].
- [24] N. Kidonakis, *Int. J. Mod. Phys. A* **19**, 1793 (2004) [hep-ph/0303186]; *Mod. Phys. Lett. A* **19**, 405 (2004) [hep-ph/0401147].
- [25] N. Kidonakis, *Phys. Rev. D* **73**, 034001 (2006) [hep-ph/0509079].
- [26] J. Kodaira and L. Trentadue, *Phys. Lett.* **112B**, 66 (1982).
- [27] N. Kidonakis, *Phys. Rev. D* **77**, 053008 (2008), arXiv:0711.0142 [hep-ph].
- [28] N. Kidonakis, *Phys. Rev. D* **64**, 014009 (2001) [hep-ph/0010002].
- [29] V. Ravindran, *Nucl. Phys. B* **752**, 173 (2006) [hep-ph/0603041].
- [30] CDF Collaboration, *Phys. Rev. Lett.* **74**, 2626 (1995) [hep-ex/9503002].
- [31] D0 Collaboration, *Phys. Rev. Lett.* **74**, 2632 (1995) [hep-ex/9503003].
- [32] W. Wagner, *Rept. Prog. Phys.* **68**, 2409 (2005) [hep-ph/0507207].
- [33] R. Kehoe, M. Narain, and A. Kumar, *Int. J. Mod. Phys. A* **23**, 353 (2008), arXiv:0712.2733 [hep-ex].
- [34] N. Kidonakis and R. Vogt, *Phys. Rev. D* **68**, 114014 (2003) [hep-ph/0308222].
- [35] N. Kidonakis, E. Laenen, S. Moch, and R. Vogt, *Phys. Rev. D* **64**, 114001 (2001) [hep-ph/0105041].
- [36] A.D. Martin, R.G. Roberts, W.J. Stirling, and R.S. Thorne, *Eur. Phys. J. C* **28**, 455 (2003) [hep-ph/0211080].
- [37] CDF Collaboration, *Phys. Rev. Lett.* **96**, 202002 (2006) [hep-ex/0603043]; *Phys. Rev. D* **74**, 072006 (2006) [hep-ex/0607035]; *Phys. Rev. D* **74**, 072005 (2006) [hep-ex/0607095]; *Phys. Rev. D* **76**, 072009 (2007), arXiv:0706.3790 [hep-ex].
- [38] D0 Collaboration, *Phys. Rev. D* **74**, 112004 (2006) [hep-ex/0611002]; *Phys. Rev. D* **76**, 072007 (2007) [hep-ex/0612040]; *Phys. Rev. D* **76**, 092007 (2007), arXiv:0705.2788 [hep-ex]; *Phys. Rev. D* **76**, 052006 (2007), arXiv:0706.0458 [hep-ex].
- [39] D0 Collaboration, *Phys. Rev. Lett.* **98**, 181802 (2007) [hep-ex/0612052].

- [40] CDF Collaboration, *Conf. Note* 8964; *Conf. Note* 8968.
- [41] N. Kidonakis, *Phys. Rev. D* **74**, 114012 (2006) [hep-ph/0609287].
- [42] N. Kidonakis, *Phys. Rev. D* **75**, 071501(R) (2007) [hep-ph/0701080].
- [43] N. Kidonakis, *Acta Phys. Polon. B* **39**, 1593 (2008), arXiv:0802.3381 [hep-ph].
- [44] A.D. Martin, R.G. Roberts, W.J. Stirling, and R.S. Thorne, *Phys. Lett. B* **604**, 61 (2004) [hep-ph/0410230].
- [45] B.W. Harris, E. Laenen, L. Phaf, Z. Sullivan, and S. Weinzierl, *Phys. Rev. D* **66**, 054024 (2002) [hep-ph/0207055].
- [46] S.H. Zhu, *Phys. Lett. B* **524**, 283 (2002) [hep-ph/0109269]; (E) *B* **537**, 351 (2002).
- [47] P.B. Arnold and M.H. Reno, *Nucl. Phys. B* **319**, 37 (1989); (E) *B* **330**, 284 (1990).
- [48] R.J. Gonsalves, J. Pawlowski, and C.-F. Wai, *Phys. Rev. D* **40**, 2245 (1989); *Phys. Lett. B* **252**, 663 (1990).
- [49] R.J. Gonsalves, N. Kidonakis, and A. Sabio Vera, *Phys. Rev. Lett.* **95**, 222001 (2005) [hep-ph/0507317].
- [50] N. Kidonakis and A. Sabio Vera, *JHEP* **02**, 027 (2004) [hep-ph/0311266].
- [51] Particle Data Group, S. Eidelman *et al.*, *Phys. Lett. B* **592**, 1 (2004).
- [52] P.W. Higgs, *Phys. Rev. Lett* **12**, 132 (1964); *Phys. Rev. Lett.* **13**, 508 (1964); *Phys. Rev.* **145**, 1156 (1966); F. Englert and R. Brout, *Phys. Rev. Lett.* **13**, 321 (1964); G.S. Guralnik, C.R. Hagen, and T.W.B. Kibble, *Phys. Rev. Lett.* **13**, 585 (1964).
- [53] The Higgs Working Group: Summary Report, in *Les Houches 2003, Physics at TeV colliders*, p. 1 [hep-ph/0406152], and references therein.
- [54] R.V. Harlander and W.B. Kilgore, *Phys. Rev. D* **68**, 013001 (2003) [hep-ph/0304035].
- [55] M. Kramer, E. Laenen, and M. Spira, *Nucl. Phys. B* **511**, 523 (1998) [hep-ph/9611272].
- [56] N. Kidonakis, in *DPF 2004, Int. J. Mod. Phys. A* **20**, 3726 (2005) [hep-ph/0410116].
- [57] A.D. Martin, W.J. Stirling, R.S. Thorne, and G. Watt, *Phys. Lett. B* **652**, 292 (2007) [arXiv:0706.0459].
- [58] S. Catani, F. Fiorani, and G. Marchesini, *Phys. Lett. B* **234**, 339 (1990).
- [59] G. Marchesini, *Nucl. Phys. B* **445**, 49 (1995) [hep-ph/9412327].
- [60] M. Ciafaloni, *Nucl. Phys. B* **296**, 49 (1988).

- 
- [61] S. Catani, F. Fiorani, G. Marchesini, and G. Oriani, *Nucl. Phys. B* **361**, 645 (1991).
  - [62] J.R. Forshaw and A. Sabio Vera, *Phys. Lett. B* **440**, 141 (1998) [hep-ph/9806394].
  - [63] J.R. Forshaw, A. Sabio Vera, and B.R. Webber, *J. Phys. G* **25**, 1511 (1999) [hep-ph/9812318].
  - [64] B.R. Webber, *Phys. Lett. B* **444**, 81 (1998) [hep-ph/9810286].
  - [65] C. Ewerz and B.R. Webber, *JHEP* **04**, 022 (1999) [hep-ph/9904244].
  - [66] C. Ewerz and B.R. Webber, *JHEP* **08**, 019 (1999) [hep-ph/9907430].
  - [67] G.P. Salam, *JHEP* **03**, 009 (1999) [hep-ph/9902324].
  - [68] M. Dittmar *et al.*, arXiv:hep-ph/0511119.
  - [69] S. Alekhin *et al.*, arXiv:hep-ph/0601012.
  - [70] S. Alekhin *et al.*, arXiv:hep-ph/0601013.
  - [71] J.R. Andersen *et al.* [Small  $x$  Collaboration], *Eur. Phys. J. C* **48**, 53 (2006) [hep-ph/0604189].
  - [72] J.R. Andersen and A. Sabio Vera, *Phys. Lett. B* **567**, 116 (2003) [hep-ph/0305236].
  - [73] J.R. Andersen and A. Sabio Vera, *Nucl. Phys. B* **679**, 345 (2004) [hep-ph/0309331].
  - [74] J.R. Andersen and A. Sabio Vera, *Nucl. Phys. B* **699**, 90 (2004) [hep-th/0406009].
  - [75] J.R. Andersen and A. Sabio Vera, *JHEP* **01**, 045 (2005) [hep-ph/0411231].
  - [76] J. Bartels, A. Sabio Vera, and F. Schwennsen, *JHEP* **11**, 051 (2006) [hep-ph/0608154].
  - [77] G.P. Salam, *JHEP* **07**, 019 (1998) [hep-ph/9806482].
  - [78] A. Sabio Vera, *Nucl. Phys. B* **722**, 65 (2005) [hep-ph/0505128].
  - [79] F. Caporale, A. Papa, and A. Sabio Vera, *Eur. Phys. J. C* **53**, 525 (2008), arXiv:0707.4100 [hep-ph].
  - [80] A. Sabio Vera, *Nucl. Phys. B* **746**, 1 (2006) [hep-ph/0602250].
  - [81] A.H. Mueller and H. Navelet, *Nucl. Phys. B* **282**, 727 (1987).
  - [82] V. Del Duca and C.R. Schmidt, *Phys. Rev. D* **49**, 4510 (1994) [hep-ph/9311290].
  - [83] V. Del Duca and C.R. Schmidt, *Phys. Rev. D* **51**, 2150 (1995) [hep-ph/9407359].
  - [84] W.J. Stirling, *Nucl. Phys. B* **423**, 56 (1994) [hep-ph/9401266].

- [85] S. Abachi *et al.* [D0 Collaboration], *Phys. Rev. Lett.* **77**, 595 (1996) [hep-ex/9603010].
- [86] B. Abbott *et al.* [D0 Collaboration], *Phys. Rev. Lett.* **84**, 5722 (2000) [hep-ex/9912032].
- [87] B. Abbott *et al.* [D0 Collaboration], *Phys. Rev. Lett.* **80**, 666 (1998) [hep-ex/9707016].
- [88] F. Abe *et al.* [CDF Collaboration], *Phys. Rev. Lett.* **77**, 5336 (1996) [hep-ex/9609011]; (E) **78**, 4307 (1997).
- [89] L.N. Lipatov, *Sov. Phys. JETP* **63**, 904 (1986) [*Zh. Eksp. Teor. Fiz.* **90**, 1536 (1986)].
- [90] J. Bartels, D. Colferai and G.P. Vacca, *Eur. Phys. J. C* **24**, 83 (2002) [hep-ph/0112283].
- [91] J. Bartels, D. Colferai and G.P. Vacca, *Eur. Phys. J. C* **29**, 235 (2003) [hep-ph/0206290].
- [92] A.V. Kotikov and L.N. Lipatov, *Nucl. Phys. B* **582**, 19 (2000) [hep-ph/0004008].
- [93] A. Sabio Vera and F. Schwennsen, *Nucl. Phys. B* **776**, 170 (2007) [hep-ph/0702158].
- [94] C. Marquet and C. Royon, arXiv:0704.3409 [hep-ph].
- [95] A. Sabio Vera and F. Schwennsen, *Phys. Rev. D* **77**, 014001 (2008), arXiv:0708.0549 [hep-ph].